

2B Dupl

PUR-73-108-E  
E-0002

JUL 12 1973

Experiment #2B

NDHEP 73-9 (Revised)  
May, 1973  
W. D. Shephard  
J. M. Bishop  
E. Fokitis

Magnetic Field of the 30-inch Hydrogen Bubble Chamber at NAL:

Report on Results of Fringe-Field Measurements and

Central-Field Measurements

Notre Dame-Toronto\*

## I. Introduction.

During the period from December 19, 1972 to January 7, 1973 an extensive program of measurements of the fringe field of the 30-inch HBC magnet at NAL was carried out. Measurements of two components of the field were made at approximately 1900 points in the fringe field downstream from the bubble chamber at each of two magnet currents (nominal currents were 18,000 and 16,000 amps). An additional 800 measurements were made to determine the effects on the field of iron phototube shields used with a  $dE/dx$  counter installed in the downstream magnet slot as

---

### \*Participants in measurements of the field include:

University of Notre Dame - J. M. Bishop, N. N. Biswas, N. M. Cason, R. L. Erichsen, E. Fokitis, V. P. Kenney, V. Polychronakos, W. L. Rickhoff, W. D. Shephard, and T. Thornsen;

University of Toronto - M. Goddard, D. Harrison, W. Jackson, R. Jones, G. Levman, G. J. Luste, J. Martin, P. Patel (McGill Univ.), and J. D. Prentice.

Other participants included:

R. Walker, National Accelerator Laboratory and R. Diamond, University of Wisconsin.

R. E. Juhala, National Accelerator Laboratory, provided some of the equipment for the measurements.

part of experiment 2B. Measurements were also made at about 180 points in the fringe field upstream from the bubble chamber in the region traversed by incident beams of particles. In addition about 200 measurements were made in the visible volume of the chamber to check the calibration of the field, the accuracy of existing field maps, and the variation of the central field with magnet current.

This report describes the equipment used in the acquisition of the data and provides estimates of the precision with which the measurements of field and of position could be made. The reduction of the raw data to a form useful for obtaining fits to the fringe field is discussed. Simple plots of the fringe field in regions traversed by beam and secondary particles are provided and a polynomial approximation for the fringe field is discussed. This may be used as an approximation in estimating the effects of the fringe field on secondary particles from interactions in the chamber. Plots are also provided which allow an estimation of the bending of incident particles prior to entering the chamber. We also discuss studies made at Notre Dame on the variation of the central field with magnet current and on the applicability of currently available parameterizations of the field in the visible volume of the chamber.

The raw measurements have been transcribed onto magnetic tape. Transformations of the raw data to yield corrected field components and coordinates in either beam-line-based or magnet-based coordinate systems are discussed in detail. If detailed knowledge of the field measurements,

is needed at this time transcriptions of the data tape can be provided by either the University of Notre Dame or the University of Toronto.

A modified polynomial subroutine for the magnetic field in the visible region of the chamber which fits our measurements and includes the observed scaling of the field with magnet current is available from Notre Dame. The preliminary polynomial parametrization of the fringe field described in Section III. E. may be used as an approximation to the upstream and downstream fringe fields.

## II. Apparatus and Procedure.

### A. Experimental Apparatus.

The magnetic field was measured with Hall probes which were positioned at accurately determined locations by means of a precision measuring device designed by R. L. Erichsen and constructed at Notre Dame. The measuring device was designed to allow accurate positioning of the probes at points on a 1" x 1" x 1" grid over a basic volume as large as 6" high by 12" wide by 5'6" long. It was based on a modification of the conventional "hole-plate" system. The basic device is sketched in Fig. 1. A long stainless steel boom moves through linear bearings mounted in a milled block. The boom is drilled with a series of holes (precision < 2 mils) so it can be pinned to the block over a range of positions determined by its length. The pin also prevents the boom and the probe holder from rotating with respect to the block. The bearing block is mounted by means of 4 precision positioning pins on a base plate drilled with a grid of holes.

The block can be positioned at 1" intervals to < 2 mils on a line running across the plate. Spacers milled to < 1 mil tolerance in thickness allow a variation of up to 6" in the height of the boom with respect to the plate. The plate is mounted on a strong-back frame and levelled to < 1 mil/foot. The frame can be supported and levelled at a series of heights in a large frame rigidly mounted with respect to the magnet. A sketch of the overall system is shown in Fig. 2. Targets are mounted on the plate, bearing block, and probe holder so that their positions could be surveyed each time the plate was moved. Deflection of the boom as a function of probe position was mapped independently and corrections were determined. The sensitive areas of the Hall probes were carefully positioned in a lucite probe holder which could be precision mounted on booms of various lengths to cover an extended range of positions. A standard magnet was used to check the orthogonality of the probes with respect to each other and their orientation with respect to the probe holder. After alignment they were locked in position. The overall accuracy of probe position for measurements made with the base plate at a single position is estimated at < 20 mils. Limitations on the accuracy with which the position of the base plate could be determined when it was moved in height increase the uncertainty in probe position over a larger volume but the accuracy is still estimated to be < 40 mils. Further details about the measuring device are contained in the Notre Dame internal report NDHEP 72-15 by W. D. Shephard and R. Erichsen.

The Hall probes and gaussmeters used in the measurement were provided by Roland Juhala of NAL. The major component of the field ( $B_z$ ) was measured with a Bell HTL 8-0608 transverse Hall probe connected via a matched calibrated 10 ft. extension cable, to a Bell 810 Gaussmeter. The gaussmeter output was displayed on a digital voltmeter. The probe has a range of 30 kilogauss and is guaranteed linear to better than 0.25% without calibration. A calibration curve for this probe was available and was used to correct the readings as a function of the field. Temperature stability was better than .13 gauss/ $^{\circ}$ C. The active area was nominally 0.040" in diameter. The second component of the fringe field ( $B_x$ ) was measured with a Bell SAK4-1808 Hall probe connected via a matched 10 ft. extension cable to a Bell 640 gaussmeter with output displayed on a digital voltmeter. The probe has a range of 10 kilogauss and a linearity of better than 0.25%. No calibration curve was available for this probe.

Before the probes were mounted in the probe holder the probe-gaussmeter systems were zeroed and the readings were checked against readings of an NMR probe in the field of a standard magnet mounted in the cross gallery at NAL. Agreement was excellent (.04% difference at 4800 gauss). The standard magnet was also used to position the probes in the probe holder so the sensitive areas were parallel to the machined faces of the holder and orthogonal to each other.

#### B. Procedure for Determining Positions.

A major problem in obtaining an accurate map of the 30" HBC fringe

field lies in determining the positions of the Hall probe relative to the magnet with high precision. This is of great importance since the field gradient may be as large as  $\sim 1.3$  kilogauss/in. Measurements taken with the base plate of the measuring device in a single position lie on a grid with relative positions established to better than 20 mils. One must also determine the absolute position of the base plate with respect to a reference coordinate system each time the plate is moved and must relate the reference coordinate system to the magnet and bubble chamber. The uncertainty in the latter determination is the largest uncertainty in our position determinations. Since R. Walker of NAL and R. Diamond of Wisconsin were engaged in surveying the positions of the wide-gap spark chambers of Experiment 2B they agreed to help in our survey to determine the position of the magnet-measuring system. Much of the procedure we used was developed by R. Walker, who has also taken responsibility for much of the reduction of the survey data necessary to obtain positions in a Cartesian coordinate system.

The only survey marks available for reference were tied to a coordinate system based on the nominal beam line. This "beam-line" system was chosen as the reference coordinate system. Measurements were also made to determine the exact position of the bubble-chamber magnet with respect to this coordinate system to allow a later specification of coordinates in a magnet-based or chamber-based coordinate system. All surveying for the fringe-field maps was done with a precision theodolite supplied by R. Walker of NAL. Processing of most of the theodolite measurement data

has been done independently at Notre Dame by E. Fokitis and J. Bishop and at NAL by R. Walker. The independent results have agreed satisfactorily.

The "beam-line" coordinate system was defined as follows:

The positive X direction is chosen as the nominal beam direction (approximately North). The Z axis is horizontal and perpendicular to the beam line. Thus it is approximately parallel to the optic axes of the bubble chamber cameras and the positive direction is taken as away from the cameras (approximately East). The Y axis is vertically upward, forming a right-handed system. The origin is chosen to be directly above a punchmark on a survey plug in a line of plugs downstream from the bubble chamber. This line of plugs defines the perpendicular to the nominal beam line and the plug chosen to define the origin is on the nominal beam line. The  $Y = 0$  plane is chosen as the horizontal plane containing the center line of the magnet. A sketch of the coordinate system is shown in Fig. 3.

The magnet-based (chamber-based) coordinate system has axes approximately parallel to those of the beam-based system. The Y axis is again vertically upward. However, the Z and X axes are rotated by  $\sim 0.12^\circ$  clockwise, as viewed from above, so that they coincide with the symmetry axes of the magnet as deduced from theodolite measurements. The origin is taken as the center of the magnet which is also assumed to be center of the bubble chamber at operating temperature. This origin has the same Y coordinate as the "beam-line" system but the Z coordinate is shifted slightly and there is, of course, a large shift in the X coordinate.

The relations between the two coordinate systems and the positions of the magnet-measuring system for measuring the downstream fringe field were determined by locating the theodolite on the line of plugs perpendicular to the beam line. Its position was adjusted until the horizontal theodolite readings on the two plugs on either side of the central plug agreed within 5 sec. of arc. The Z position of the theodolite was determined by measuring the angular coordinates of two targets exactly 30" apart on a vertical precision rule suspended directly over the central plug. The magnet position relative to the theodolite was determined by measuring the angular coordinates of targets 30" apart on rulers placed horizontally and vertically on the North and East faces of the magnet. The theodolite was approximately 330" east of the beam line and angles could be determined with a least count of 1 sec. Repeated measurements were typically in agreement to better than 5 sec. of arc.

Details of the measurements used to determine the position of the base plate of the measuring apparatus will be described in Section III of this report.

The positions of the measuring apparatus for measurements of the up-stream fringe field were determined with respect to the "beam-line" coordinate system by transferring the theodolite to a position upstream from the chamber on a line defined by two survey plugs to be perpendicular to the nominal beam line. The new position of the theodolite relative to the original position was measured by placing targets on the floor of the bubble-chamber building so that they lay on a line joining the two theodolite positions

as determined with the theodolite in its original downstream position.

Details will be given in Section IV.

Positions of Hall probes for measurements of the field inside the chamber were determined by theodolite measurements made through one of the camera ports of the chamber. Measurements were made of targets attached to the probe holder and of the fiducials on the windows of the bubble chamber. These data have been processed by R. Walker with the program FIDAJUST. Transformations between the fiducial grids for the chamber at room temperature and at operating temperatures have also been obtained. Further details are given in Section V.

### III. Downstream Fringe Field.

#### A. Measurements.

For measurements of the downstream fringe field the stand supporting the probe-positioning device was mounted downstream from the magnet between the magnet and the enclosure containing the spark chambers for Exp. 2B. The frame was centered on the beam line and was braced against the platform on top of the bubble chamber to provide rigidity. Levelling screws at the base allowed small variations in the Y (vertical) position.

The base plate of the device was successively mounted at a series of heights 6" apart on the frame. At each height the plate was positioned to  $\leq 40$  mils in X and Z by centering a plumb bob over the reference punch mark on the survey plug defining the XZ origin. The position of the plate

could be adjusted and it could be locked in position by means of the bolts connecting it to the main frame. These were adjusted so that the plumb bob string was centered in a small hole in the plate when the plumb bob was directly above the reference mark. The base plate was then levelled to better than 1 mil/ft. with precision levels by adjusting the levelling screws at the base of the main frame. (Flatness of the base plate was maintained with adjusting screws holding the 3/4" x 16" x 60" aluminum plate to a support frame constructed from 2" x 4" box beams.) The theodolite was set at the approximate level of the bearing block mounted on the base plate and was carefully realigned to lie on the line of survey plugs. A precision-milled block was pinned in a standard position on the base plate and the XZ rotation of the plate was adjusted so that the boom motion was parallel to the X axis. The proper position was determined by auto-reflection from a mirror mounted on the side of the block with its face perpendicular to the boom axis.

After the plate was securely locked in position theodolite measurements were made to determine its absolute position. The bearing block was pinned to the plate in a standard position and measurements were made of a target mounted on the side of the block. The coordinates of this target with respect to the boom axis and the pin securing the boom in the block were independently determined. Measurements were also made of targets 30" apart on a rule mounted horizontally on the side of the base plate, targets on a 30" rule mounted on the East face of the magnet near

the downstream edge and a target mounted on the East face of the magnet at  $Y = 0$  near the downstream edge.

After this survey was completed measurements were made of the field at a series of points in a horizontal plane. A typical grid of points in an XZ plane is shown in Fig. 4. The bearing block was successively pinned in a series of Z positions across the plate. For each Z position the boom was pinned in a series of X positions and the readings from the transverse and axial Hall probes were recorded. For most of the runs one person positioned the boom and read aloud the DVM readings. Two people independently recorded the readings on separate data sheets and one of them repeated the readings aloud to minimize transcription errors. The space coordinates for readings were recorded in terms of nominal coordinates specified by labels mounted on the base plate and frame of the measuring device. These coordinates correspond roughly to coordinates in the "magnet-based" reference frame. Data were recorded on standard data sheets like the sample shown in Fig. 5.

Measurements for a typical XZ plane were made at X values from a nominal  $X = +20''$  (actually  $\approx +19 \frac{7}{8}''$  from chamber center-line) to  $X = +80''$ . The major component of the field typically reverses direction at about  $X = +50''$  and is usually  $\leq 50$  gauss by  $X = +80''$ . Two booms of different lengths were used to cover this range. The limit of measurements at small X values was determined by a locking pin which fixed the position of a stop at the rear of the long boom to prevent any possibility of

the probe holder touching the thin window in the chamber body. Measurements were made at Z values which varied with X as determined by obstructions within the magnet. The range was determined by clearance for the probe holder and is illustrated in Fig. 4.

After all points in a single XZ plane were measured the precision-milled spacer block under the bearing block was changed and the process was repeated. For a single base-plate position XZ planes at nominal  $\Delta Y = 0''$ ,  $+2''$ , and  $+4''$  were completely surveyed. Some points were recorded for  $\Delta Y = +6''$  for comparison with data from  $\Delta Y = 0''$  with the base plate moved  $6''$  higher.

After all data for a given base-plate position were taken, the theodolite survey was repeated to check for movement of the apparatus during the measurements and to provide redundancy for the later determination of Cartesian coordinates for the points.

The height of the base plate was then changed by a multiple of approximately  $6''$  and the process was repeated. The complete survey includes data at 5 different base-plate positions. These yield field maps in 16 XZ planes at nominal  $2''$  spacings ranging from a nominal  $Y = -20''$  (actually  $Y \approx -20 \frac{3}{8}''$ ) to a nominal  $Y = +10''$  (actually  $Y \approx +9 \frac{1}{2}''$ ) with respect to the median plane of the magnet. The location of these planes with respect to the slot in the magnet iron is sketched in Fig. 6.

Checks of field measurements within the slot at different magnet currents indicated that in some regions the field did not scale linearly with current. To provide data in case the magnet must be run below the

standard current of 18000 amps we made an additional complete map of the downstream fringe field at a nominal current of 16000 amps.

Magnet currents are recorded in terms of the shunt voltages displayed in the bubble-chamber control room. These shunt voltages were monitored frequently and were recorded for each data sheet. Additional values were recorded if drifts were noted during data-taking. Nominal shunt voltages for 18000 and 16000 amps are 45 and 40 millivolts, respectively. Shunt voltages have been specified to .01 mV . We note, however, that the meter normally indicates rapid fluctuations of order  $\pm 0.05$  mV . Long-term fluctuations were kept small by readjusting the controls whenever drifts were observed. Over the period of the measurements the shunt voltages recorded vary from 45.00 to 45.09 mV and from 39.99 to 40.08 mV . Shunt voltages for each point are included on the magnetic tape of the data.

An additional series of measurements was made to determine the effects on the fringe field of some heavy iron phototube shields which are part of a  $dE/dx$  counter which is installed in the downstream magnet slot as part of the Exp. 2B trigger. A mock-up of the counter with similar iron shields was constructed and was installed in the slot. Measurements of the field were made at about 800 points with the mock-up installed. The effect on the field was observed to be quite small except very near the shields. We conclude that the distortion of the field can be regarded as negligibly small. The data are available if further study is desired.

## B. Corrections to Field Measurements.

### 1. Linearity of the Transverse Hall Probe.

A calibration curve for the HTL8-0608 Hall probe is available and must be used to correct the raw data transcribed from the data sheets to the magnetic tape. The calibration curve is shown in Fig. 7. Corrections range from 0.0 gauss for fields less than 5 kilogauss to a positive deviation of 39 gauss at 19 kilogauss and a negative deviation of 28 gauss at 30 kilogauss as shown in the figure. A table of values which we have used with linear interpolation to compute this correction is shown in Table I.

### 2. Linearity of the Axial Hall Probe.

No correction curve was available for the SAK8-1808 Hall probe and no correction has been made. The probe specifications indicate that linearity is good to better than  $\pm 1/4\%$  without correction.

### 3. Scale Differences for Bell 810 Gaussmeter.

Two scales on the Bell 810 gaussmeter (transverse probe) were used. A consistent shift of 20 gauss was observed in switching between the 10 K (100 K) scale and the 1 K (10 K) scale with the probe in the same location. This is believed to be due to a difference in zero adjustment for the two scales caused by our initial calibration of the system. Zero adjustment was initially done on the 1 K (10 K) scale. Values for all readings made with the 10 K (100 K) scale have been corrected by -20 gauss before the data were recorded on magnetic tape.

4. Scales for Bell 640 Gaussmeter.

Only one scale was used on the Bell 640 gaussmeter. No correction was necessary.

5. Temperature Corrections.

Both probes are specified to be stable with respect to temperature variations to better than .13 gauss/ $^{\circ}$ C. The temperature near the magnet was monitored during the run and varied by  $\leq 3^{\circ}$ C. No correction was deemed necessary.

6. Mixing of  $B_x$  and  $B_y$  field components.

A slight mixing of the  $B_x$  and  $B_y$  components of the field can occur as the boom bends under its own weight shifting the sensitive area of the axial probe out of a vertical plane. This "boom droop" effect depends on the length of boom extending beyond the bearing block. While the "boom droop" is large enough that we must correct for it in our determinations of coordinates for the probes, the effect on  $B_x$  due to this mixing is estimated to be only about 1 part in  $10^3$  at most. No correction has been made since  $B_y$  was not measured.

C. Position Coordinates for Measurements.

The positions for measurements were recorded, for convenience, in terms of integers which do not correspond exactly to any absolute coordinate system. The coordinates initially recorded on the magnetic tape of the data are these nominal coordinates. We have analyzed in detail the data from the theodolite surveys used to determine the absolute positions of the base

plate. These data were reduced independently by R. Walker at NAL and by J. Bishop and E. Fokitis at Notre Dame. The results were in excellent agreement. Careful studies of the measuring apparatus have been made to relate Hall-probe positions to plate positions. Corrections have been made for effects such as "boom droop" -- the deflection of the boom due to its own weight. Coordinates of both transverse and axial probes must be specified since they are separated vertically in the probe holder by 1".

In this section we specify transformations from nominal coordinates as specified on the tape to absolute coordinates for both probes in either the "beam-line" coordinate system or the "magnet-based" coordinate system defined in Section II B of this report. Information is also provided on the direction of the field as the magnet is normally used (positive particles are bent upward in passing through the chamber) and on correcting the values of the measured field components for the relative rotation of the two standard coordinate systems. A simple FORTRAN program has been written by E. Fokitis and J. M. Bishop of Notre Dame to perform the necessary transformations on the data from the data tape and to print out tables of the raw data and the data transformed into both coordinate systems. Copies are available from Notre Dame upon request.

1. "Beam-line" Coordinates and Field Components.

In the transformations the following notation is used:

$X_0, Y_0, Z_0$  are the nominal coordinates.

$X_p, Y_p, Z_p$  are coordinates of a target on the bearing block as determined from survey data taken with the bearing block mounted in a standard position. They differ for each base-plate position and are used to modify coordinates according to base-plate position. They depend on  $Y_o$ . The spacer thickness above  $Y_p$  for a given  $Y_o$  is denoted by  $\Delta Y$ .  $X_T, Y_T, Z_T$  are coordinates of the sensitive area of the transverse probe used to measure the major component of the field.  $X_A, Y_A, Z_A$  are the coordinates of the sensitive area of the axial probe used to measure one of the small components of the field.

$DX$  is the difference between the  $X$  positions of the probes due to "boom droop".

$DY$  is the correction to  $Y$  positions of the probes due to "boom droop".

$B_T$  and  $B_A$  are transverse and axial probe readings.

$\Delta B$  is the correction to  $B_T$  for probe linearity given in Table I.

$B_z$  and  $B_x$  are components of the field in the "beam-line".

Values for  $X_p, Y_p, Z_p$  and  $\Delta Y$  as a function of  $Y_o$  are given in Table II. Values of  $DX$  and  $DY$  as a function of  $X_o$  are given in Table III. All coordinates are given in inches. The transformations from nominal to "beam-line" coordinates are as follows.

$$X_T = X_o - 131.960 + X_p(Y_o)$$

$$Y_T = Y_p(Y_o) + \Delta Y - DY$$

$$Z_T = Z_o - 6.308 + Z_p(Y_o)$$

$$X_A = X_T + DX$$

$$Y_A = Y_T - 1.000$$

$$Z_A = Z_T$$

$$B_z = -(B_T - \Delta B)$$

$$B_x = -B_A$$

## 2. Magnet-based Coordinates and Field Components.

The same notation with the addition of an asterisk (\*) is used to identify coordinates expressed in the magnet-based system. Transformations are made from "beam-line" coordinates to magnet-based (chamber-based) coordinates as follows:

$$X_T^* = X_T + 132.201 + .00211 (Z_T + .081)$$

$$Y_T^* = Y_T$$

$$Z_T^* = Z_T + .081 - .00211 (X_T + 132.201)$$

$$\begin{aligned} X_A^* &= X_A + 132.201 + .00211 (Z_A + .081) \\ &= X_T^* + DX \end{aligned}$$

$$Y_A^* = Y_A = Y_T^* - 1.000$$

$$Z_A^* = Z_A + .081 - .00211 (X_A + 132.201)$$

$$B_z^* = B_z - .00211 B_x$$

$$B_x^* = B_x + .00211 B_z$$

An examination of the transformation will show that the magnet is rotated with respect to the beam line by  $.121^\circ$  (.00211 rad) clockwise as seen from above and that the magnet center appears to be shifted  $-.081''$  in Z from the beam line. These shifts are derived from an analysis of our survey

data. As far as we can determine, the bubble chamber is believed to be centered in the magnet at operating temperatures, so chamber-based and magnet-based coordinate systems are assumed to be identical. However, the assumptions that the magnet position is known with an accuracy comparable to our accuracy in measuring coordinates in the beam-line system and that the magnet is really symmetric in the "magnet-based" coordinate system are open to question. The magnet coils themselves can be positioned within the magnet structure only to an accuracy (limited by thermal expansion etc.) which is probably no better than 1/8" to 1/4". The magnet position was determined by theodolite measurements of targets on the outside of the magnet. Even the layers of paint on the magnet are thick compared to the precision specified for our coordinate determinations. Also it is unclear whether the configuration of the magnet is highly reproducible when its halves are separated for access to the chamber and then reassembled. As shown in the next section, plots of  $B_x^*$  as a function of  $Z^*$  do not indicate exact symmetry about the  $Z^* = 0$  line in the magnet-based system. An empirical modification of the magnet-based coordinate system can be made on the basis of these measurements and will be discussed in Section III. E. In Section IV. E. it is noted that a shift of 0.1" in the  $-X^*$  direction for the center of the magnet would significantly improve the agreement between our values for the upstream and downstream fringe fields as a function of distance from the assumed vertical center line of the magnet. Further studies of the relationship of

the various coordinate systems using straight-through beam tracks in the bubble chamber and the wide-gap spark chambers of Experiment 2B are needed, as well as further survey data.

#### D. Field Tables.

As previously stated, IBM-compatible magnetic tapes at Notre Dame and at Toronto contain tabulations of the raw measurements for the downstream fringe field. A FORTRAN program is available at Notre Dame to perform corrections and to transform the data to "beam-line" and/or magnet-based coordinate systems. Requests for these can be addressed to W. D. Shephard at Notre Dame. If you wish a copy of the magnetic tape please furnish us with a blank tape which can be used for the copy and specify whether 7 track, 556 or 800 BPI, or 9 track, 1600 BPI tapes are required.

#### E. Preliminary Parametrization of the Downstream Fringe Field.

Although a detailed parametrization of the downstream fringe field using all of the data is not yet available, the shape of the field appears regular enough that, to first approximation the fringe field in the region of interest may be treated as cylindrically symmetric about the magnet (bubble chamber) axis, thus the major component,  $B_z^*$ , may be parametrized as a function of  $R^* = \sqrt{(X^*)^2 + (Y^*)^2}$ . In this section we will show some simple plots of the field shape and provide approximate parametrizations. In Fig. 8 is shown a plot of  $B_z^*$  versus  $R^*$  for our experimental points along the line closest to  $Y^* = Z^* = 0$  (actually  $Y^* \approx -0.5''$ ,  $Z^* \approx +0.3''$ ) out to  $R^* \sim 50''$ . Points are also shown for  $B_z^*$  inside the chamber from a parametrization

to be discussed in Section V. Results for 18000 and 16000 amp magnet currents are shown. The measured fringe field points extend to a minimum  $X^* \approx 20''$  ( $R^* \approx 20''$ ) and appear to connect smoothly near  $R^* = 18''$  with the plot of the field inside the chamber. However, we note again that a shift of  $+0.1''$  in  $X^*$  for the fringe-field measurements would not lead to an obvious difference in the smoothness of the connection near  $R^* = 18''$ . By  $X^* \approx 50''$  the field has dropped to approximately zero. Studies of  $B_z^*$  versus  $R^*$  for other experimental lines of points indicate that  $B_z^*$  at a fixed  $R^*$  varies only slightly with  $Y^*$  and  $Z^*$  within the magnet slot. The largest variations of  $B_z^*$  with  $R^*$  occur in the  $R^* = 40''$  to  $R^* = 50''$  range near the outer radius of the coil where the field has already decreased considerably in magnitude. This may be seen in Fig. 9a, where values of  $B_z^*$  along various lines of measured points have been plotted as a function of  $R^*$  for  $40'' < R^* \leq 80''$ . In this plot may also be seen the variation of  $B_z^*$  with  $R^*$  at 18000 amps from  $R^* = 50''$  to  $R^* = 80''$  where the field is quite small and has reversed direction.

Since the data shown in Figs. 8 and 9 appear to provide a reasonable approximation of the downstream fringe field in the region traversed by fast secondary tracks from interactions in the chamber, we have fitted these points with power series in  $R^*$ . Fits were made to the measurements at points near the  $Z^* = 0$ ,  $Y^* = 0$  line. The fits, obtained by N. N. Biswas of Notre Dame, are of the form:

$$B_z^* = \sum_{n=0}^5 a_n (R^* - R_0^*)^n .$$

This form for the polynomial was selected in order to make the fits converge rapidly. The values of  $R_0^*$  were arbitrarily chosen to lie near the center of the  $R^*$  range for which the fit was being made. The number of terms in the polynomial was chosen to provide fits of acceptable accuracy. Separate fits were performed for two ranges of  $R^*$  for both 16000 amp and 18000 amp magnet currents. The data for  $14'' < R^* < 50''$  were fitted, with  $R_0^*$  chosen to be  $35''$ . In these fits to 19 points the rms deviation and maximum deviation of the fit from the measurements were respectively 83.5 gauss and 163 gauss at 18000 amp, and 81.2 gauss and 167 gauss at 16000 amp. The fits are shown as solid curves in Fig. 8. They provide a good approximation to the fringe field over the range of the fit. For  $R^* > 50''$  the fits described above yield values of  $B_z^*$  which rapidly diverge from the measured values, as can be seen in Fig. 9b where the fit for 18000 amp is shown as the dashed curve plotted on an expanded scale.

For most purposes the magnetic field for  $R^* > 50''$  can be neglected; the resulting error in  $\int B dl$  is estimated to be less than 1% for a typical secondary track. For completeness, however, we have made polynomial fits of the same form in the region  $48'' < R^* < 80''$ , with  $R_0^*$  chosen to be  $60''$ . In these fits to 13 points the rms deviation and maximum deviation of the fit from the measurements were respectively 11.4 gauss and 26.9 gauss at 18000 amp, and 11.0 gauss and 25.4 gauss at 16000 amp. The fit for 18000 gauss is shown as the solid curve on Fig. 9b. These fits begin to diverge for  $R^* > 80''$ , but there the field is certainly negligible. No attempt was

made to parametrize the variation of the field with  $Y^*$  and  $Z^*$  at fixed  $R^*$ . As can be seen in Fig. 9a, this variation is clearly apparent in the region  $40'' < R^* < 50''$ , but the resultant variation in  $\int B dl$  for the fringe-field region is estimated to be less than about 1% for fast forward secondary tracks from beam interactions in the bubble chamber. If better fits are required for a specific purpose, the fringe-field measurements on the magnetic tape described in Section III. D. are available for fitting.

The coefficients  $a_n$  for the fits described above are listed in Table IV. These fits together with the central-field subroutine described in Section V. H., may be used to determine the magnetic field in the region traversed by fast secondary tracks downstream from the chamber. We suggest using the central-field subroutine for the region  $R^* < 18''$ , the fits with  $R_0^* = 35''$  for the region  $18'' \leq R^* < 47.5''$ , and the fits with  $R_0^* = 60''$  for the region  $47.5'' \leq R^* \leq 80''$ . For  $R^* > 80''$  one may assume all field components to be zero. Alternatively one may use the fits with  $R_0^* = 35''$  for the region  $18'' \leq R^* \leq 50''$  and assume the field to be zero for  $R^* > 50''$  with little loss in accuracy. The suggested representation of the field exhibits small discontinuities at  $R^* = 18''$ ,  $47.5''$ , and  $80''$  but the effect of these should be insignificant in current experiments. A conservative estimate indicates that the suggested parametrization of the field will yield values of  $\int B dl$  for fast forward particles which are accurate to better than 1% over the range  $18'' < R^* < 80''$ .

The polynomial fits may be used to estimate  $\int B dl$  for fast forward

secondary tracks. For example, along the line  $Y^* = Z^* = 0$ ,  $\int B_z^* dR^*$  would be 11.4 kG-m in the visible region of the chamber ( $0'' \leq R^* \leq 15''$ ) and 13.7 kG-m in the fringe-field region ( $15'' \leq R^* \leq 80''$ ) for a total of 25.1 kG-m at a magnet current of 18000 amp. The corresponding numbers at 16000 amp are 10.3 kG-m in the central region and 12.5 kG-m in the fringe-field region for a total of 22.8 kG-m. This illustrates again the importance of the downstream fringe field for hybrid-spectrometer experiments, since more than half of the total  $\int B dl$  is outside the visible region of the bubble chamber for a particle formed in the center of the chamber.

The fits described above may also be used to calculate an approximate representation of the small components of the field. This approximation should be sufficiently accurate for current experiments since it indicates that  $\int B_y^* dl$  will be less than 2% of  $\int B_z^* dl$  for all cases of interest. If we assume cylindrical symmetry for the field about  $R^* = 0$  and assume that the field is symmetric about  $Z^* = 0$ , then the requirement that  $\vec{\nabla} \times \vec{B} = 0$  may be used together with the fit of  $B_z^*(R^*)$  to provide an estimate of  $\partial B_r^* / \partial Z^*$ . We have then:

$$\frac{\partial B_r^*}{\partial Z^*} = \frac{\partial B_z^*}{\partial R^*} = \sum_{n=1}^5 n a_n (R^* - R_o^*)^{n-1}$$

Then, with the assumption of symmetry about  $Z^* = 0$

$$B_r^*(R^*, Z^*) = Z^* \frac{\partial B_z^*}{\partial R^*}$$

and

$$B_x^* = B_r^* \cos \phi$$

$$B_y^* = B_r^* \sin \phi$$

where  $\tan \phi = Y^*/X^*$ .

The magnitude of  $\partial B_z^*/\partial R^*$  calculated in this manner varies with  $R^*$  up to a maximum of about 1.3 kG/inch as shown in Fig. 10. Studies of experimental values for  $B_x^*$  indicate that this parametrization provides a reasonably good estimate of the small components of the field. They also suggest, however, that our "magnet-based" coordinate system is not exactly the coordinate system in which the field exhibits symmetry about  $Z^* = 0$ . Some curves of  $B_x^*$  versus  $Z^*$  for various  $R^*$  near  $Y^* = 0$  are shown in Fig. 11 for data taken at 18000 amps. In view of the assumptions which must be made about the magnet and the way in which its position was determined it does not seem surprising that we do not get  $B_x^* = 0$  exactly at  $Z^* = 0$  in the system defined as the magnet-based system on the basis of survey data. Probably the best way to correct for this is to determine empirically a "field-based" coordinate system (indicated by primes) in which the data do give  $B'_x \approx 0$  at  $Z' = 0$ . This has been done approximately. The result is a system which is rotated from the "beam-line" system by 1.031 degrees counterclockwise as seen from above and the center is shifted -0.41" in Z from the beam line. Transformations from "beam-line" coordinates to this empirical "field-based" system are:

$$X'_T = X_T + 132.201 + .0180 (Z_T + .410)$$

$$Y'_T = Y_T$$

$$Z'_T = Z_T + .410 - .0180 (X_T + 132.201)$$

$$X'_A = X'_T + DX$$

$$Y'_A = Y'_T - 1.000$$

$$Z'_A = Z'_T$$

$$B'_z = B_z - .0180 B_x$$

$$B'_x = B_x + .0180 B_z$$

Further refinement of this transformation would be required for a precision fit to the complete set of fringe-field data if the fit assumes symmetry about  $Z = 0$ .

The values of  $\partial B'_x / \partial Z'$  near  $Y' = 0$  calculated from the experimental data are found to be approximately independent of  $Z'$  over the width of the slot in the magnet and are roughly consistent with the values estimated from our polynomial fit to  $B_z^*$ . This is illustrated in Fig. 12. It should be emphasized that the major component of the field,  $B_z$ , is affected very little by our choice of the "magnet-based" or "field-based" coordinates defined above. However, a shift of our coordinate system parallel to the X axis could have a significant effect on  $B_z$  as a function of R in the region of interest.

F. Modification of the Downstream Fringe Field by the dE/dx Counter of Experiment 2B.

A supplementary study was made to determine whether the dE/dx counter installed in the downstream magnet slot as part of the Experiment 2B trigger produces a significant modification of the downstream fringe

field. A mockup of the  $dE/dx$  counter with similar iron phototube shields was constructed by R. Erichsen of Notre Dame and was installed in the magnet slot. Measurements at about 800 points within the slot indicated that the distortion of the field was insignificant except at positions quite near the shields. We concluded from the raw measurements that the effects of the counter on the shield may safely be neglected in current experiments. No further study of these data is planned, but the data sheets are available if needed.

#### IV. Upstream Fringe Field

##### A. Measurements.

After completion of the downstream fringe field measurements the stand for the probe-positioning device was moved to the upstream side of the bubble chamber and braced in position. Because of the construction of the frame surrounding the bubble chamber the frame was about 4" further from the magnet. The stand was again centered approximately on the beam line and the plate was successively mounted at two different heights, levelled, rotated so the boom moved parallel to the beam-line and surveyed in position. As discussed in Section II. B. the theodolite was transferred to a position upstream from the chamber. The new position for the theodolite was carefully correlated with the original position and with the position of targets on the floor of the bubble-chamber building. Measurements were again made of targets and rules fastened to the side of the magnet to help in relating the various surveys.

Readings of the transverse and axial Hall probes for the upstream fringe field for a nominal magnet current of 18000 amps were made at a series of  $X$  values along 9 lines. Again the coordinates for the points were specified in terms of nominal coordinates read from labels on the base plate and frame. The nominal coordinates again were assigned so that they corresponded roughly to the coordinates for a "magnet-based" system although the correspondence was less exact than for the downstream measurements. In particular the direction of the  $Z$  axis was reversed from that used for the nominal coordinates in the downstream data. Measurements were made along lines at nominal coordinates  $Y_0 = 0, \pm 2''$  and  $Z_0 = 0, \pm 2''$ . In terms of a "magnet-based" coordinate system these correspond approximately to lines at  $Y^* = -1.2'', -3.2''$  and  $-5.1''$  and  $Z^* = -2'', 0''$  and  $+2''$ . This is approximately the region traversed by beams of particles incident on the chamber. For a given  $Y_0$ , measurements were made at  $X$  values starting at  $X_0 = 28''$  ( $X^* \approx -27.7''$ ) for  $Z_0 = 0$ ,  $X_0 = 30''$  ( $X^* \approx -29.7''$ ) for  $Z_0 = +2''$ , and  $X_0 = 36''$  ( $X^* \approx -35.7''$ ) for  $Z_0 = -2''$ . Measurements were made out to  $X_0 = 68''$  ( $X^* \approx -67.7''$ ). The recording process was similar to that which was used in the downstream survey. Measurements were made at about 180 points.

## B. Corrections to Field.

### 1. Linearity of the Transverse Hall Probe.

The same correction to  $B_T$  should be made for the upstream measurements as is described in Section II. B. 1. and tabulated in Table I.

2. Linearity of the Axial Hall Probe.

Again, no correction can be made. (See Section II. B. 2.)

3. Scale Change for Bell 810 Gaussmeter.

All upstream readings were taken on the 1K (10K) scale of the Bell 810 gaussmeter so no corrections are necessary. (See Section II. B. 3.)

4. Scale Change for Bell 640 Gaussmeter.

No correction is necessary. (See Section II. B. 4.)

5. Temperature Corrections.

No corrections are necessary. (See Section II. B. 5.)

6. Mixing of  $B_x$  and  $B_y$  Field Components.

No significant correction is necessary. (See Section II. B. 6.)

C. Position Coordinates for Measurements.

An initial reduction of the theodolite survey data for the upstream fringe field measurements has been made so that we can compare the upstream and downstream fringe fields in a magnet-based coordinate system. Preliminary results are available. The transformations based on the preliminary data yield results which suggest that the upstream fringe field is of the same shape as the downstream fringe field. However, the  $B_z^*$  versus  $R^*$  curve for the upstream data is shifted in  $R^*$  by about 0.2" as will be shown in Section IV. E. It seems probable that this indicates a need for more careful checks on the position measurements rather than a true difference in fringe-field magnitude. Some slight differences might result due to the differences in the dimensions of the slot in the magnet

iron. The upstream slot is 12" wide and extends 24" above and below  $Y = 0$ , while the downstream slot is 10" wide and extends 17" above and 31" below the chamber center line  $Y = 0$ . It seems improbable, however that this would account for the observed shift. As noted in Section III, a shift in  $X$  of about 0.1" for the magnet center would remove the discrepancy.

The preliminary transformations from nominal coordinates and field components to coordinates and field components, in a magnet-based system for the upstream fringe-field data are:

$$X_T^* = - (X_O + .659) - .00211 (Z_O + .105)$$

$$Y_T^* = Y_O - 3.244 - DY \text{ for } y_O = 0, +2$$

and

$$Y_T^* = Y_O - 3.168 - DY \text{ for } Y_O = -2$$

where

$$DY = DY (|X_O - 8|) \text{ from Table III}$$

$$Z_T^* = -(Z_O + .105) + .00211 (X_O + .659)$$

$$X_A^* = X_T^* - DX$$

where

$$DX = DX (|X_O - 8|) \text{ from Table III}$$

$$Y_A^* = Y_T^* - 1.000$$

$$Z_A^* = Z_T^*$$

$$B_z^* = (B_T - \Delta B) - .00211 B_A$$

$$B_x^* = + B_A + .00211 B_T$$

These transformations should be improved by further study.

#### D. Field Tables.

We plan to add the upstream fringe-field data as a separate file on the magnetic tape described in Section III. D.

### E. Preliminary Parameterization of the Upstream Fringe Field.

In Fig. 13 are shown some data points from the upstream fringe field measurements with  $B_z^*$  plotted against  $R^*$  using the preliminary transformations of Section IV. C. Also shown is the parameterization of the downstream field described in Section III. E. The shape of the upstream fringe field is seen to be quite similar to the shape for the downstream field but there is an apparent change in magnitude. As previously discussed, the differences could be accounted for by a change of 0.2" in the  $X^*$  values for the upstream measurements or by a change of 0.1" in the  $X^*$  coordinate assumed for the magnet center. As a first approximation we suggest using the same parameterization for the upstream field as is described in Section III. E. for the downstream field.

## V. Central Field. (Field in Visible Region of Bubble Chamber.)

### A. Measurements.

It seemed most desirable to make some measurements of the magnetic field inside the visible region of the bubble chamber under the same conditions for which the fringe field measurements were made. These are also the conditions under which the chamber is normally operated at NAL, except, of course, for the fact that the chamber was at room temperature. In addition to making measurements at a number of points in a plane which is approximately the central plane of the chamber at nominal magnet currents of 18000 and 16000 amps, we selected a single location in the chamber (about 10" below center near  $X = Z = 0$ ) where the field was near the

maximum magnitude we could observe and systematically varied the current in the magnet in nominal steps of 1000 amps (2.5 mV steps in shunt voltage) from 18000 amps (shunt reading 45.06 mV) down to 4000 amps (shunt reading 10.06 mV) while recording the readings of the transverse and axial Hall probes. This has allowed us to study the variation of the magnetic field with magnet current in the visible region of the chamber. An additional series of readings of the field at a line of points at various Y coordinates near  $X = Z = 0$  was made with the magnet current reduced to zero. The residual field was measured to be less than 2 gauss at all the points.

The only access to the visible region of the chamber at the time of the survey was through the three small piston ports in the top of the chamber. In order to make measurements through the piston ports a special set of holes was precision-drilled in the base plate used in the fringe field measurements to allow the bearing block to be mounted on the plate at right angles to its normal position in three locations such that the boom and probe holder could be lowered through the piston ports when the base plate was mounted vertically on edge on the top of the chamber. The drilling was done by machinists in the 15 ft. bubble chamber machine shop. A mounting system was devised by R. Erichsen of Notre Dame which enabled the plate to be mounted rigidly in position above the piston holes. The plate was mounted and levelled with precision levels so that its milled edge was horizontal to better than 1 mil/ft. A precision square was used in conjunction with

the levels to position the plate so its milled face was vertical to an accuracy of a few mils per foot. The boom and probe-holder assembly were successively lowered through each of the three piston holes and pinned in a series of positions at 2" spacing. In this configuration the transverse Hall probe was mounted so it provided readings of the major component of the field,  $B_z$ . The axial probe provided readings for one of the small components of the field  $B_y$ . The position of the points for  $B_z$  varied from  $Y \approx -10''$  to  $Y \approx +20''$  along lines near X-values of  $-9.7$ ,  $+1.3$  and  $+12.3''$  in a plane near  $Z \approx 0$ , in a coordinate system similar to the magnet-based system used for fringe-field measurements. For each of the three lines of points, measurements were made successively at 18000 and at 16000 amps. In addition, measurements were made of the magnetic field along the central line with the magnet turned off and of the magnetic field as a function of magnet current at the lowest point in the central line. The alignment and level of the base plate were checked each time the bearing block was moved.

In order to determine the positions of the probe holder and Hall probes within the bubble chamber a special theodolite survey was made. The theodolite was mounted in front of one of the camera ports for the bubble chamber (the "-X, -Y" camera port). J. Hunckler of the NAL Survey Group surveyed the angular positions of two targets mounted on the probe holder at known distances from the sensitive areas of the Hall probes for a number of positions of the probe holder within the chamber. He also measured the angular

positions of the fiducials on the inside surfaces of the warm chamber windows as well as autoreflexion angles from the front and back surfaces of the windows. These data have been processed by R. Walker of NAL with the program FIDAJUST which is regularly used to obtain surveys of fiducial positions in the 30" bubble chamber. This survey yielded probe positions with respect to the fiducial positions on the warm chamber window. A later survey has been made of fiducial positions when the chamber is cold. This has also been processed by R. Walker with FIDAJUST and provides us with transformations which allow us to specify the positions at which field measurements were made in the standard bubble chamber coordinate system. With the assumption that the chamber is centered in the magnet at operating temperatures, this should correspond to our "magnet-based" coordinate system except for the fact that the standard bubble-chamber coordinate system used with TVGP has the origin located in the plane of the center fiducial on the inside of the chamber window closest to the cameras rather than in the central plane of the chamber.

#### B. Corrections to Field Measurements.

Corrections to field measurements due to the characteristics of the Hall probes etc. are the same as those described in Section III. B. for the downstream fringe field measurements. Since the boom was mounted vertically for the central field measurements no corrections to either coordinates or field measurements are required to account for "boom droop".

Corrections are necessary to obtain good values for the rectangular components of the field in a magnet-based coordinate system. These are required since our results indicate that the probes were not exactly oriented normal to the  $Y^*$  and  $Z^*$  axes. From the theodolite survey data and the results of FIDAJUST we have calculated that the transverse probe was tilted at an angle of 14 mrad with respect to the fiducial plane of the warm front window. From a study of the measured values of " $B_z$ " and " $B_y$ " we estimate that the probes must have been tilted by an angle of 34 mrad with respect to the XY plane of the magnet. This is based on the assumption that  $B_y$  should vanish in the median plane of the magnet. It implies a 20 mrad tilt of the warm window with respect to the magnet. These angles appear reasonable in magnitude in light of the procedure used in aligning the measurement system for the central-field measurements. Perhaps the best justification is that we have been able to obtain excellent fits to the field in the central region of the chamber.

#### C. Position Coordinates for Measurements.

The results of the surveys and of measurements on the position of the probes with respect to the targets mounted on the probe holder have been used to provide transformations from nominal probe coordinates used in recording the field measurements to coordinates in a magnet-based or chamber-based coordinate system. These transformations include the calculated motion of the chamber and the windows and fiducials when the chamber is cooled to operating temperature.

Details of the transformations will not be given here. They lead to a table of coordinates for the 47 positions of the probes at which field measurements were made.

D. Field Tables.

The measured field components and coordinates for our measurements of the central field in the 30" bubble chamber have been written in a separate file on the magnetic tape of the survey data in use at Notre Dame (See Section III. D.

E. Parametrizations of the Central Field in the Visible Region of the Bubble Chamber.

We have compared our measurements of the central field with previous parametrizations of the field which were available to us. They include:

1. A three-component magnetic field parametrization routine initially obtained from the University of Wisconsin in 1965 and subsequently used with TVGP at Ohio University starting in 1968.
2. A one-component field routine used at Notre Dame with a version of HGEOM and an identical one-component field routine obtained from the present Argonne version of TVGP. (These are the same as 1. for  $B_z$ .)

The field subroutines give fair agreement ( $\pm 1\%$ ) with our measurements for  $B_z$  over the chamber volume when an appropriate scaling of the field was made to correspond with the magnet current at which the chamber is operated at NAL. In these parametrizations  $B_z$  varies by about 1% over

the visible region of the chamber in the plane in which our measurements were made. This is consistent with the measurements.

J. M. Bishop of Notre Dame has studied the field routines and has found that a still better fit to our measurements may be obtained by modifying one term in the polynomial for  $B_z$  from a  $+R^6$  term to a  $-R^2 X^4$  term. The agreement of  $B_z$  with our measurements is then excellent —  $\pm 0.05\%$  in the central region of the chamber to  $\pm 0.1\%$  near the edges, for both the 18000 amp and 16000 amp fields with appropriate scaling. This term is not included in the polynomials for  $B_x$  and  $B_y$ . No modification has been made to the polynomials for  $B_x$  and  $B_y$  since all our measurements were near the central plane of the magnet and provided little information about the minor components of the field. We note that the  $B_z$  calculated from this routine connects smoothly with our measurements of the downstream fringe field as shown in Fig. 8 as well as fitting our measurements of the central field.

#### F. Scaling of Central Field with Magnet Current.

From the maps of the field in the chamber at 18 kA and 16 kA and from measurements of  $B_z$  versus shunt voltage at  $X \approx Z \approx 0$  and  $Y \approx -23$  cm, we have determined the scaling of the field with current. One parametrization fits our measurements to within  $\pm 0.7\%$  over the full range of shunt voltages from 10 mV (4 kA) to 50 mV (20 kA). Another parametrization fits the measurements to within  $\pm 0.1\%$  over the range from 40 mV (16 kA) to 45 mV (18 kA). The resulting equations are given in Table V, for the

parametrizations. Also included are two earlier parametrizations of the scaling made at Wisconsin and at Toronto, which have similar dependence on current but with constants differing by up to 10%. Figure 14 shows our data and fits and those from Wisconsin and Toronto. The field shown for 20 kA is from the 1968 measurement of E. C. Berrill, as reported in a University of Toronto memo. We have modified the TVGP field routine to use the second scaling equation.

The central value of the field for 18 kA current is  $-29.747$  kG, i. e., in the negative Z direction (such that a positive beam is bent up).

#### G. Residual Field in the Magnet.

We have also measured  $B_z$  and  $B_y$  along Y near  $X = Z = 0$  for zero current, and record a residual field of less than 2 gauss.

#### H. Central Field Subroutine.

As noted in Sections V. E. and F. a polynomial subroutine for calculating the field in the visible region of the chamber has been modified by J. M. Bishop of Notre Dame to provide excellent agreement with our field measurements. This routine also includes the parametrization discussed in Section V. F. for scaling the field with magnet current. Listings and decks of the routine can be obtained from Notre Dame in a form suitable for use with TVGP. This routine, in combination with the polynomial approximation to the fringe field described in Section III. E. provides the best parametrization now available for determining  $B$  and  $\int B dl$  along the trajectories of high-momentum particles leaving the bubble chamber through the downstream slot in the magnet.

## VI. Acknowledgements

We wish to thank Dr. L. Voyvodic and the operating crews of the 30" bubble chamber for their cooperation, assistance and advice during the fringe-field measurements at NAL. The 15' bubble chamber machine shop performed vital modifications to the measuring device during the course of the run. Rough measurements of the fringe field reported earlier by Drs. I. A. Pless, R. K. Yamamoto and J. Wolfson were helpful in formulating plans for our measurements. Mr. A. Horvath and the staff of the Notre Dame Physics Department constructed the measuring device described in this report and made major contributions to the design. The downstream fringe field data were transcribed onto magnetic tape at the University of Toronto. Most of the calculations described in this report were performed at the University of Notre Dame Computing Center.

Figures

- Fig. 1. Sketch of the precision base-plate, bearing block, boom and probe-holder assembly used for mapping the fringe field of the 30" bubble-chamber magnet.
- Fig. 2. Sketch of the overall fringe-field measuring system as it was mounted downstream from the 30" bubble chamber.
- Fig. 3. Sketch of the coordinate systems with respect to beam line and magnet as used for the fringe-field mapping of the 30" bubble-chamber magnet.
- Fig. 4. A typical grid of points in an XZ plane at which measurements of the downstream fringe field were made is shown in relation to a plan view of the magnet.
- Fig. 5. Sample data sheet used for recording fringe-field measurements.
- Fig. 6. Sketch showing the side view of the magnet. The locations of planes at which the downstream fringe field was mapped are indicated.
- Fig. 7. Calibration curve for linearity corrections used with the HTL8-0608 transverse Hall probe.
- Fig. 8. Plots of  $B_z^*$  as a function of  $R^*$  near  $Y^* = Z^* = 0$  for downstream fringe field measurements at 16,000 and 18,000 amps. The curves are fits described in Section III. E.
- Fig. 9. a) Measurements of  $B_z^*$  are shown as a function of  $R^*$  in the range  $40'' < R^* < 80''$  along various lines of points at different

$Y^*$  and  $Z^*$  for 18000 amp magnet current. The solid curve is the polynomial fit to  $B_z^*(R^*)$  in the region  $18'' < R^* < 50''$ ; The dashed curve is the fit in the region  $48'' < R^* < 80''$ .

b) Measurements of  $B_z^*$  along the line  $Y^* = Z^* = 0$  are shown on an expanded scale in the region  $46'' < R^* < 80''$  together with the polynomial fits to the data in the regions  $18'' < R^* < 50''$  (dashed curve) and  $48'' < R^* < 80''$  (solid curve).

Fig. 10. Plots of  $\partial B_z^* / \partial R^*$  as a function of  $R^*$  calculated from the fits to  $B_z^*(R^*)$  described in Section III, E.

Fig. 11. Plots of  $B_x^*$  versus  $Z^*$  near  $Y^* = 0$  are shown for various values of  $R^*$ . The data were taken at a magnet current of 18000 amp.

Fig. 12. Experimental values of  $\partial B_x' / \partial Z'$  for various values of  $R'$  near  $Y' = 0$  are compared with values estimated from the polynomial fit to  $B_z^*(R^*)$  described in Section III, E. Data are shown for a magnet current of 18000 amp.

Fig. 13. Experimental points for  $B_z^*(R^*)$  for upstream fringe field measurements are shown together with a curve representing measurements of  $B_z^*(R^*)$  for the downstream fringe field measurements.

Fig. 14. Plots of various parametrizations of  $B_0/I$  as a function of  $I$  in the central region of the 30'' bubble-chamber magnet are shown together with measured values. The fits are described in Section V. F.

Table I.

Linearity Corrections for the Bell HTL8-0608  
Transverse Hall Probe.

Field Reading $B_T$ (kilogauss)	Correction $\Delta B$ (gauss)
5	0.0
6	4.0
7	7.5
8	12.0
9	16.0
10	20.0
11	24.0
12	25.0
13	30.0
14	33.0
15	36.0
16	37.0
17	38.0
18	39.0
19	39.0
20	37.0
21	36.0
22	34.0
23	29.0
24	23.0
25	18.0
26	13.0
27	5.0
28	- 4.0
29	-15.0
30	-28.0
31	-45.0

Table II.

Coordinates of Bearing-Block Target and Spacer-Block Thickness as a Function of  $Y_0$  for Downstream Fringe Field Measurements. \*

Magnet Current (amperes)	$Y_0$ (inches)	$\Delta Y$ (inches)	$X_p$ (inches)	$Y_p$ (inches)	$Z_p$ (inches)
18000	+ 10	+ 6	-0.354	+3.636	+6.279
	+ 8	+ 4			
	+ 6	+ 2			
	+ 4	0			
	+ 2	+ 4			
	0	+ 2			
	- 2	0			
16000 and 18000	- 4	+ 4	-0.375	-8.317	+6.264
	- 6	+ 2			
	- 8	0			
	- 10	+ 4			
	- 12	+ 2			
	- 14	0			
	- 16	+ 4			
- 18	+ 2				
- 20	0				
16000	+ 10	+ 6	-0.408	+3.729	+6.355
	+ 8	+ 4			
	+ 6	+ 2			
	+ 4	+ 0			
	+ 2	+ 4			
	0	+ 2			
	- 2	0			

\* See Section III. C. for definitions of these quantities.

Table III.

Values of DY and DX as a Function of  $X_0$ :

"Boom-Droop" Correction Factors\*

$X_0$ (inches)	DY (inches)	DX (inches)
20	0.260	0.009
22	0.232	0.008
24	0.210	0.007
26	0.192	0.006
28	0.174	0.006
30	0.162	0.005
32	0.150	0.005
34	0.139	0.005
36	0.130	0.004
38	0.122	0.004
40	0.113	0.003
42	0.104	0.003
44	0.096	0.003
46	0.086	0.002
48	0.082	0.002
50	0.077	0.002
52	0.072	0.001
54	0.068	0.001
56	0.064	0.001
58	0.060	0.000

\* See Section III. C. for definitions of these quantities.

Table IV.

Coefficients  $a_n$  in Fits<sup>†</sup> to the Downstream Fringe Field of the Form

$$B_z^* = \sum_{n=0}^5 a_n (R^* - R_o^*)^n$$

Magnet Current (amps)	R* Range (inches)	R <sub>o</sub> *	n	a <sub>n</sub>
18000	18-47.5	35	0	-0.129184 E+02
			1	+0.131586 E+01
			2	-0.625151 E-03
			3	-0.154600 E-02
			4	-0.239346 E-04
			5	-0.289016 E-06
18000	47.5-80	60	0	0.172518 E+00
			1	-0.201247 E-02
			2	0.953592 E-03
			3	0.310314 E-04
			4	-0.162015 E-04
			5	0.585228 E-06
16000	18-47.5	35	0	-0.117638 E+02
			1	+0.119190 E+01
			2	-0.470860 E-03
			3	-0.141781 E-02
			4	-0.212045 E-04
			5	-0.219468 E-06
16000	47.5-80	60	0	0.107172 E+00
			1	-0.225821 E-02
			2	0.865197 E-03
			3	0.376704 E-04
			4	-0.144209 E-04
			5	0.507296 E-06

† The fits are described in Section III. E. R\* and R<sub>o</sub>\* are in inches and B<sub>z</sub>\* is in kilogauss.

Note:

$$B_R^*(R^*, Z^*) = Z^* \sum_{n=1}^5 n a_n (R^* - R_o^*)^{n-1}$$

For R\* > 80 inches, both B<sub>z</sub>\* and B<sub>R</sub>\* are negligible in magnitude.

Table V.

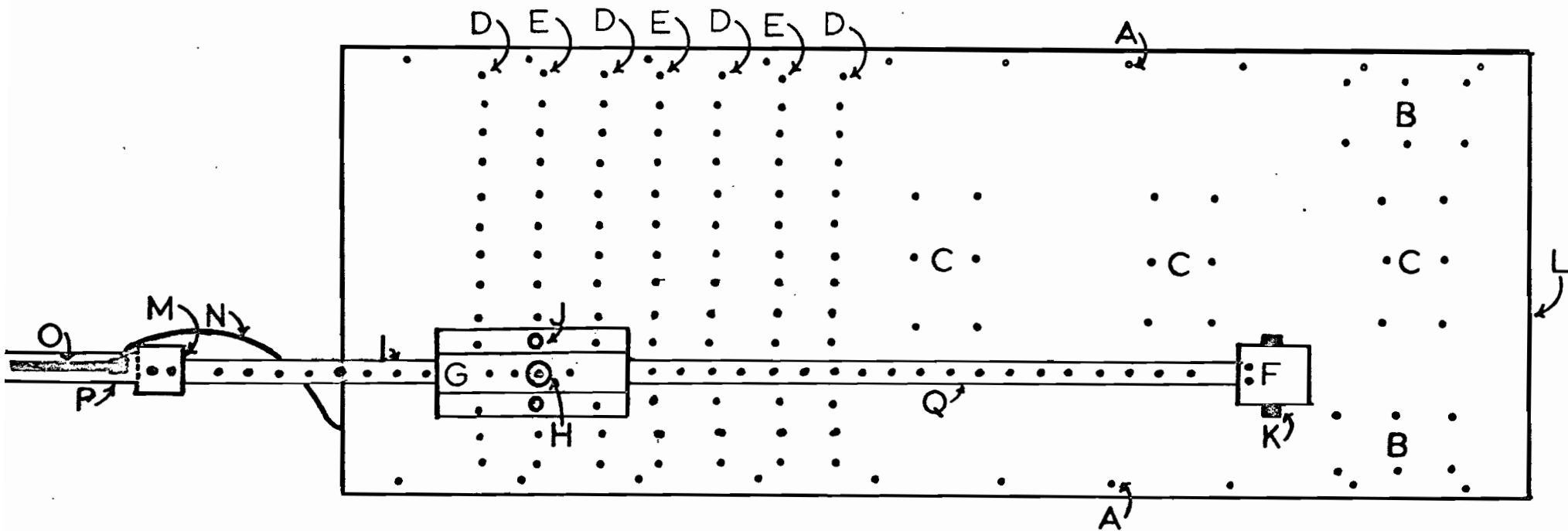
Field versus Current Inside the 30" Chamber  
 B in kG, I in kA, V in mV  
 $I = V/2.5005$

	Equation	Range	Error
1.	$B_o/I = 1.92325 - 0.01512 I$	13kA - 18kA (a) 4kA - 20kA (b)	$\pm 0.2\%$ (a) $\pm 0.7\%$ (b)
2.	$B_o/I = 1.905174 - 0.0141024 I$	16kA - 18kA (a) 12kA - 20kA (b)	$\pm 0.06\%$ (a) $\pm 0.4\%$ (b)
3.	$B_o/I = 1.89851 - 0.013878 I$	18.4 kA - 20kA	
4.	$B_o/I = 2.00835 - 0.0190874 I$	18.6kA - 20kA	

Notes:

1. J. M. Bishop, Notre Dame, 4/73; determined from measurement of B versus I at one point in chamber, over wide range of I.
2. J. M. Bishop, Notre Dame, 4/73; determined from field maps at 16kA and 18kA.
3. Memo by D. Harrison, Toronto, 7/31/68.
4. Memo by M. Firebaugh and J. Lynch, Wisconsin, 3/1/69; determined from  $K^0$  decay fits.

- (a) Range of fit and error.
- (b) Range of application and error.



- A - Levelling Screws
- B - Auto-Collimating Block Hole Pattern
- C - Piston Measurement Hole Pattern
- D - X-Axis Alignment Hole Pattern
- E - Bearing Block Holddown Threaded Holes
- F - Guide Block and Counter Weight
- G - Bearing Block
- H - Alignment Pin
- I - Stainless Steel Rod
- J - Mounting Screws
- K - Roller Bearings
- L - 3/4" Tool Plate AL

- M - Probe Adapter
- N - Probe Cable
- O - Hall Probe
- P - Probe Holder
- Q - Z-Axis Alignment Holes

30" MAGNET FIELD  
MAPPING JIG

Figure 1

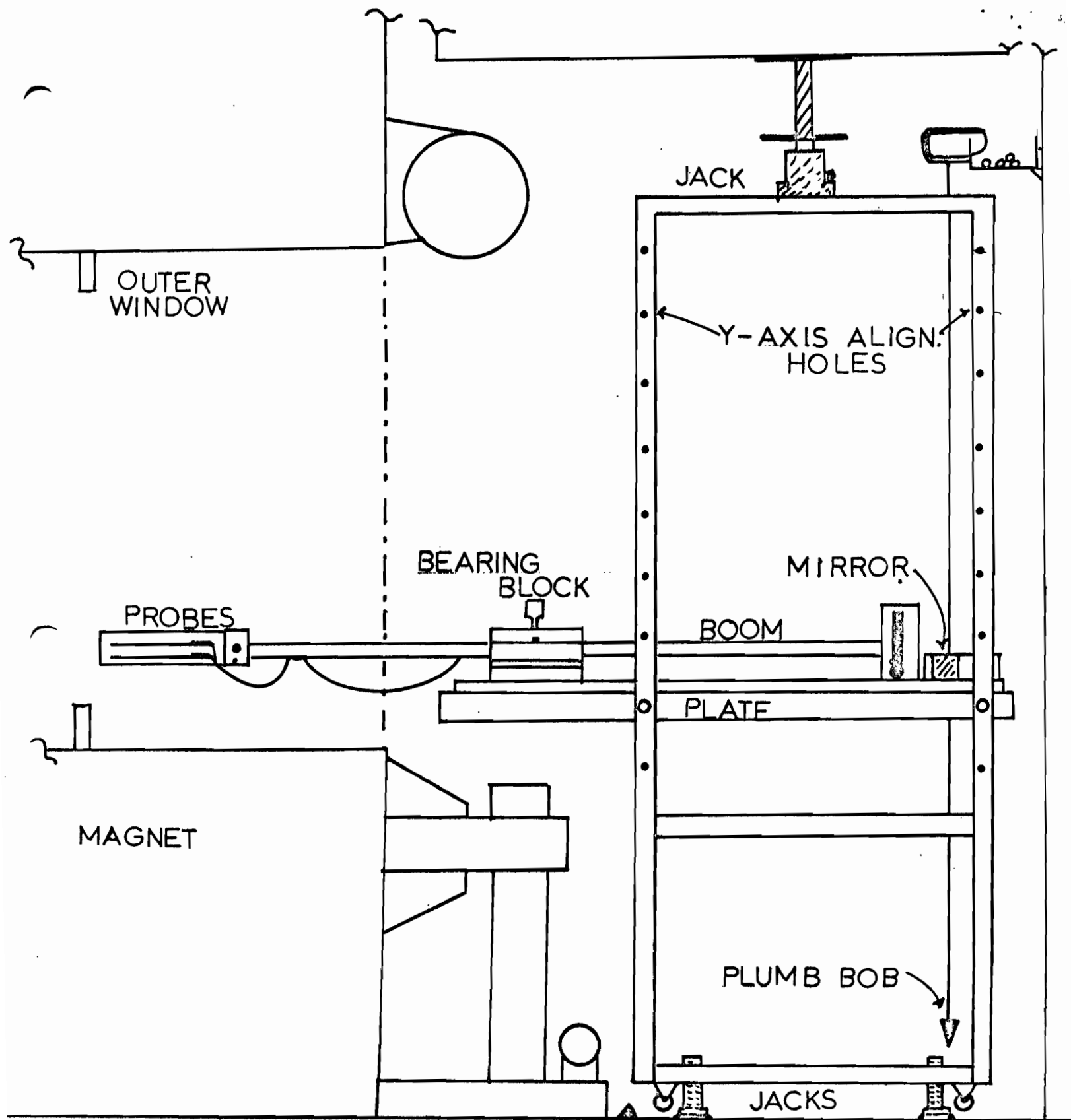


Figure 2

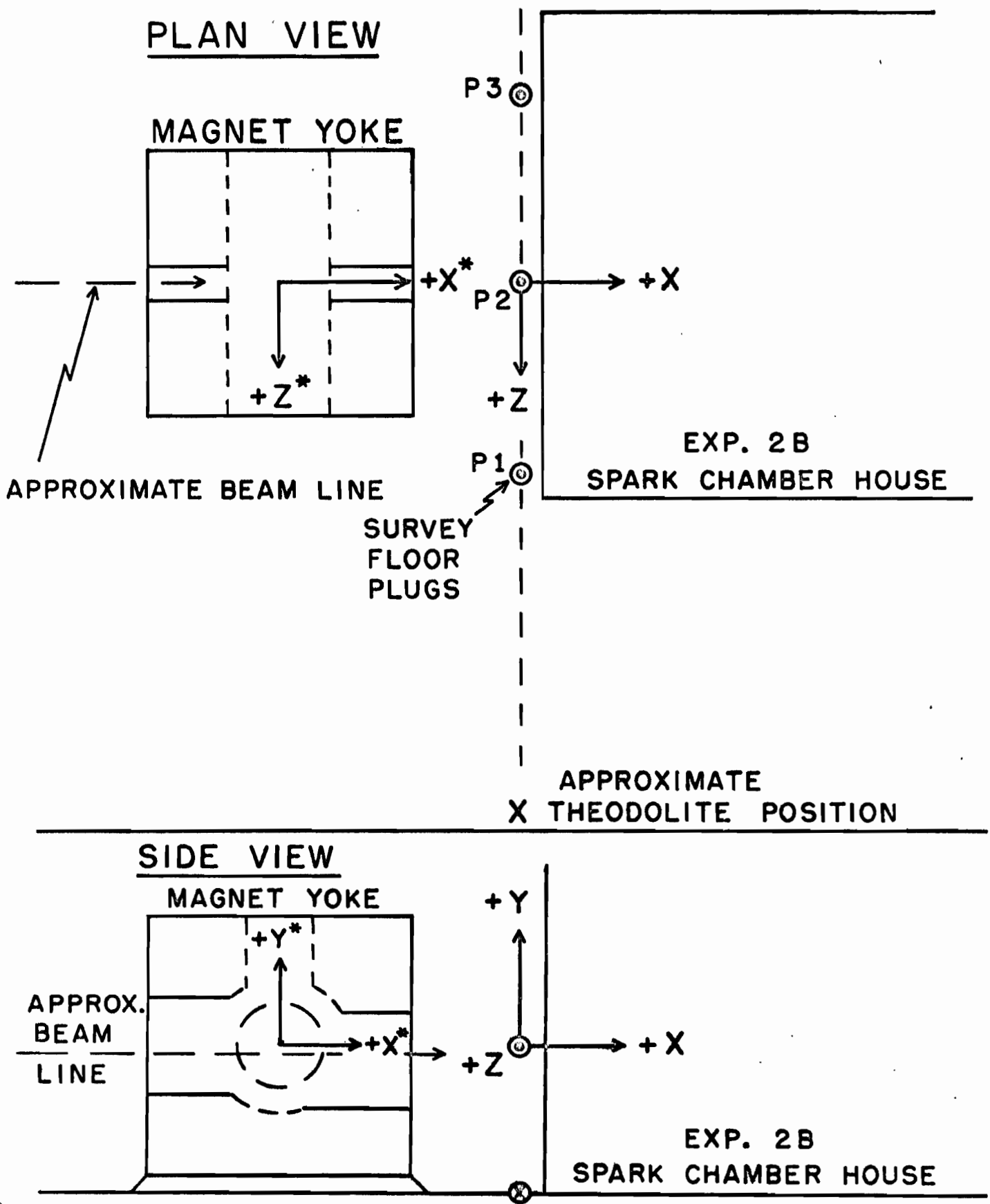


Figure 3

HORIZONTAL SECTION AT  $Y_0 = 0$

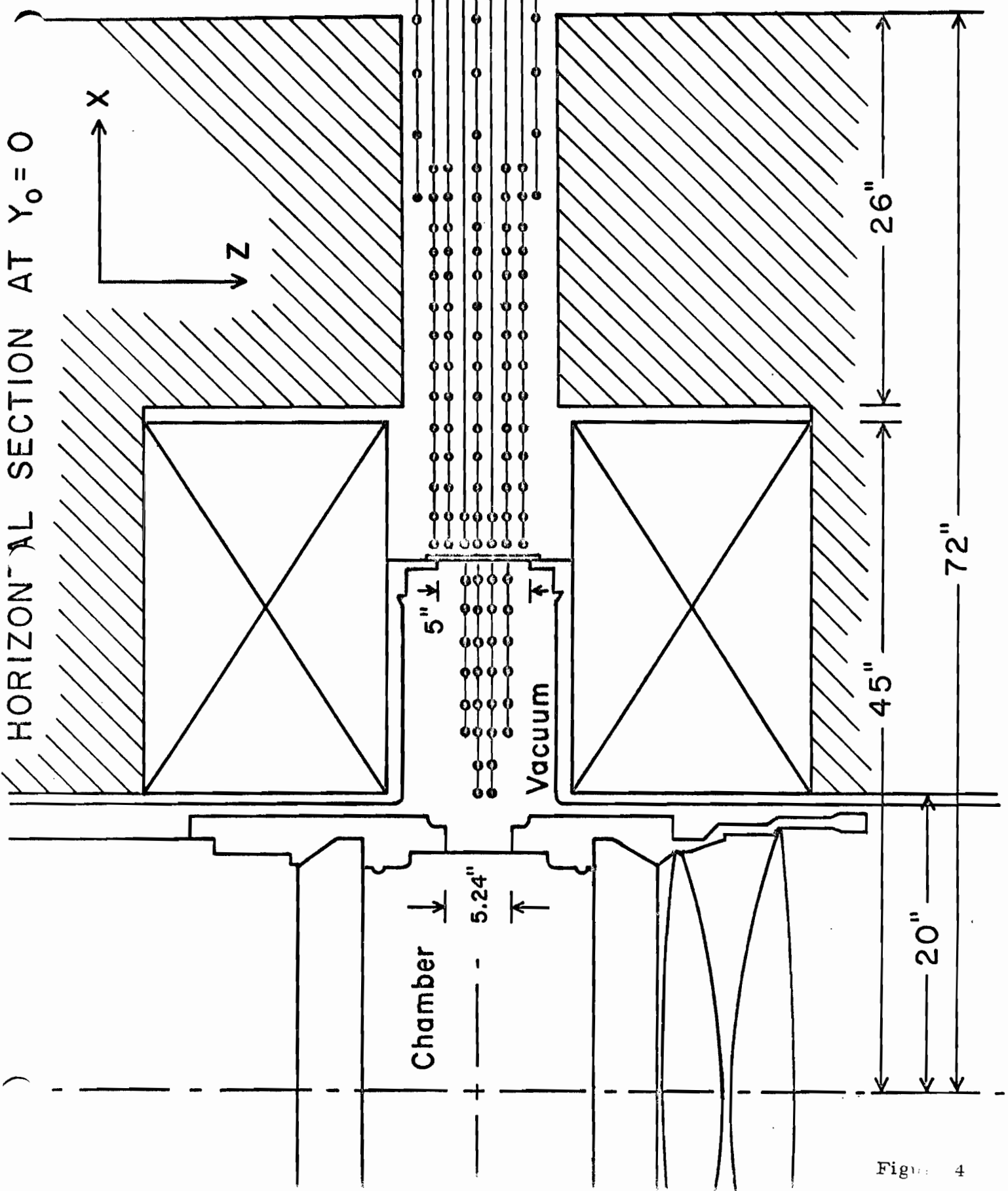


Figure 4

# 30" B.C. MAG. FIELD

Rechner - Bisuris

## Measurement

Shift crew Enrichson, Thomson  
Bisuris, Scholfield

Date 12/28/72  
Time started 13:25  
Time ended

Value of Y = 3.0  
Current = 45.05 amp  
1.05

X(Nom)	Z = -4		Z = -3		Z = -2		Z = -1		Z = 0		Z = 1		Z = 2		Z = 3	
	Bz	Bx	Bz	Bx	Bz	Bx	Bz	Bx	Bz	Bx	Bz	Bx	Bz	Bx	Bz	Bx
18																
20																
22																
24																
26																
28																
30																
32																
34																
36																
38																
40																
42																
44																
46																
48																
50																
52																
54																
56																
58																
60																
62																

X(Nom)	Z = -4		Z = 0		Z = 4	
	Bz	Bx	Bz	Bx	Bz	Bx
60						
64						
68						
72						
76						
80						
84						

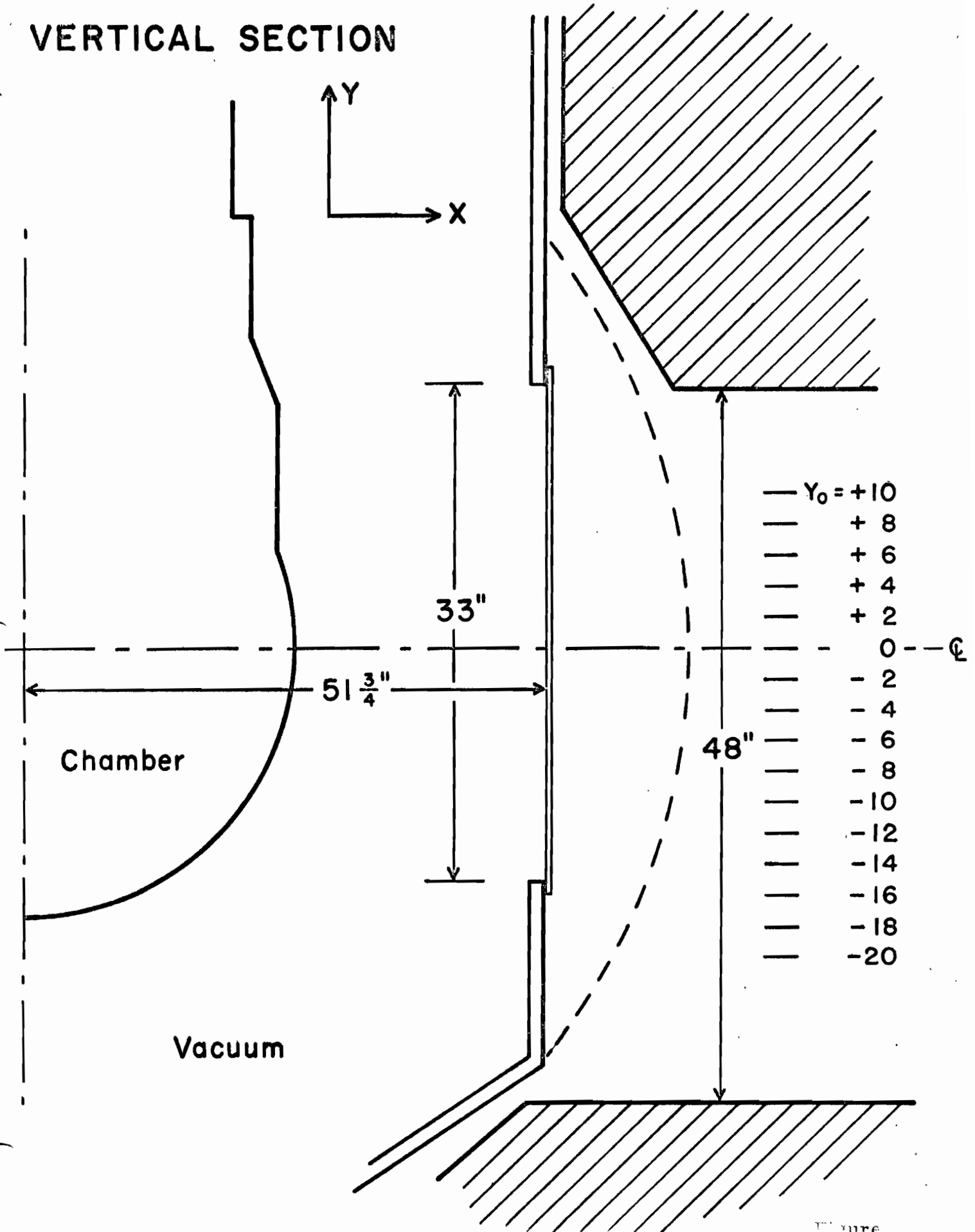
X-Probe REVERSE  
Z-Probe NORMAL

\* Range changed

T = 20°C

Figure 5

# VERTICAL SECTION



NO. HTL 8 - 0608

LINEARIZING RESISTOR,  $R_{lin} = \underline{500 \Omega}$

DATE: 12-13-72 INITIALS E.A.M.

INPUT RESISTANCE,  $R_{in} = \underline{1.35 \Omega}$

SENSITIVITY CONSTANT,  $\gamma_B = \underline{0.836 \text{ mV/kG}}$

OUTPUT RESISTANCE,  $R_{out} = \underline{\frac{.97}{1.2V} \Omega}$

CONTROL CURRENT,  $I_c = 100 \text{ mA}$

PROBE MODEL NO. HTL8-0608

HALL PROBE LINEARITY DEVIATION PLOT

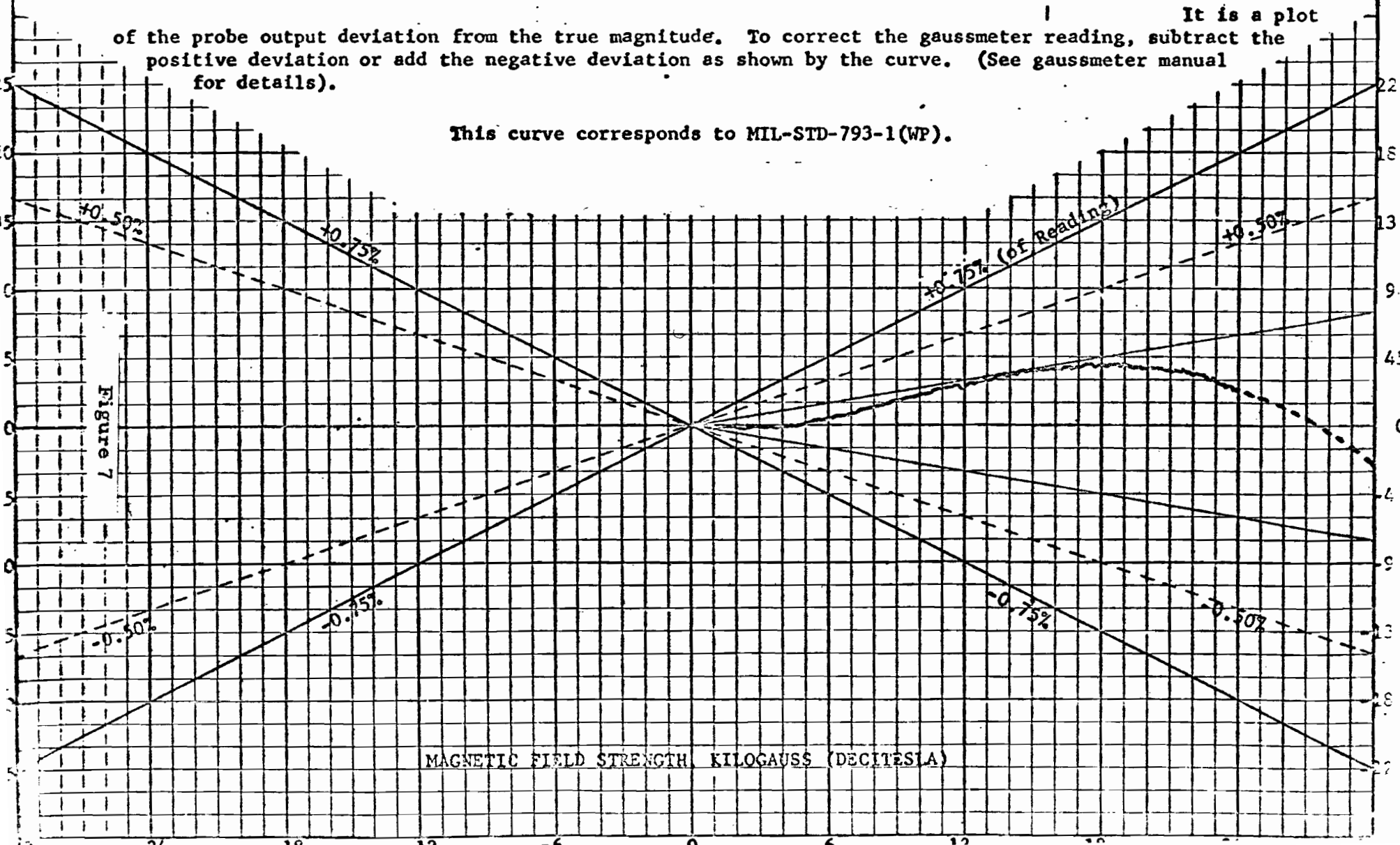
F. W. BELL, INC.  
COLUMBUS, OHIO U. S. A.  
DRAWING UA 2014

PROBE SERIAL NO. 77601

PROBE CAL. NO. 0.6748

It is a plot of the probe output deviation from the true magnitude. To correct the gaussmeter reading, subtract the positive deviation or add the negative deviation as shown by the curve. (See gaussmeter manual for details).

This curve corresponds to MIL-STD-793-1(WP).



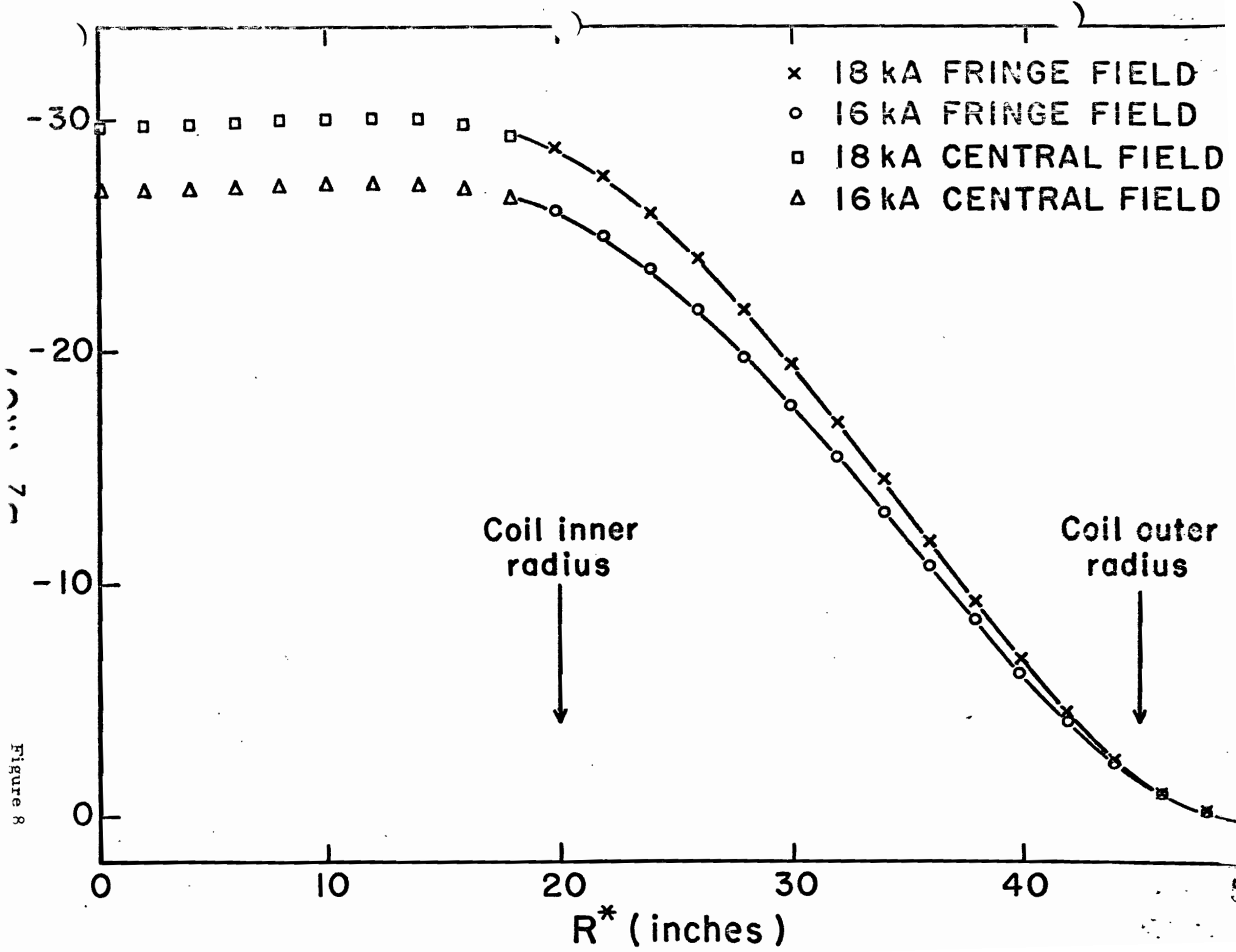


Figure 8

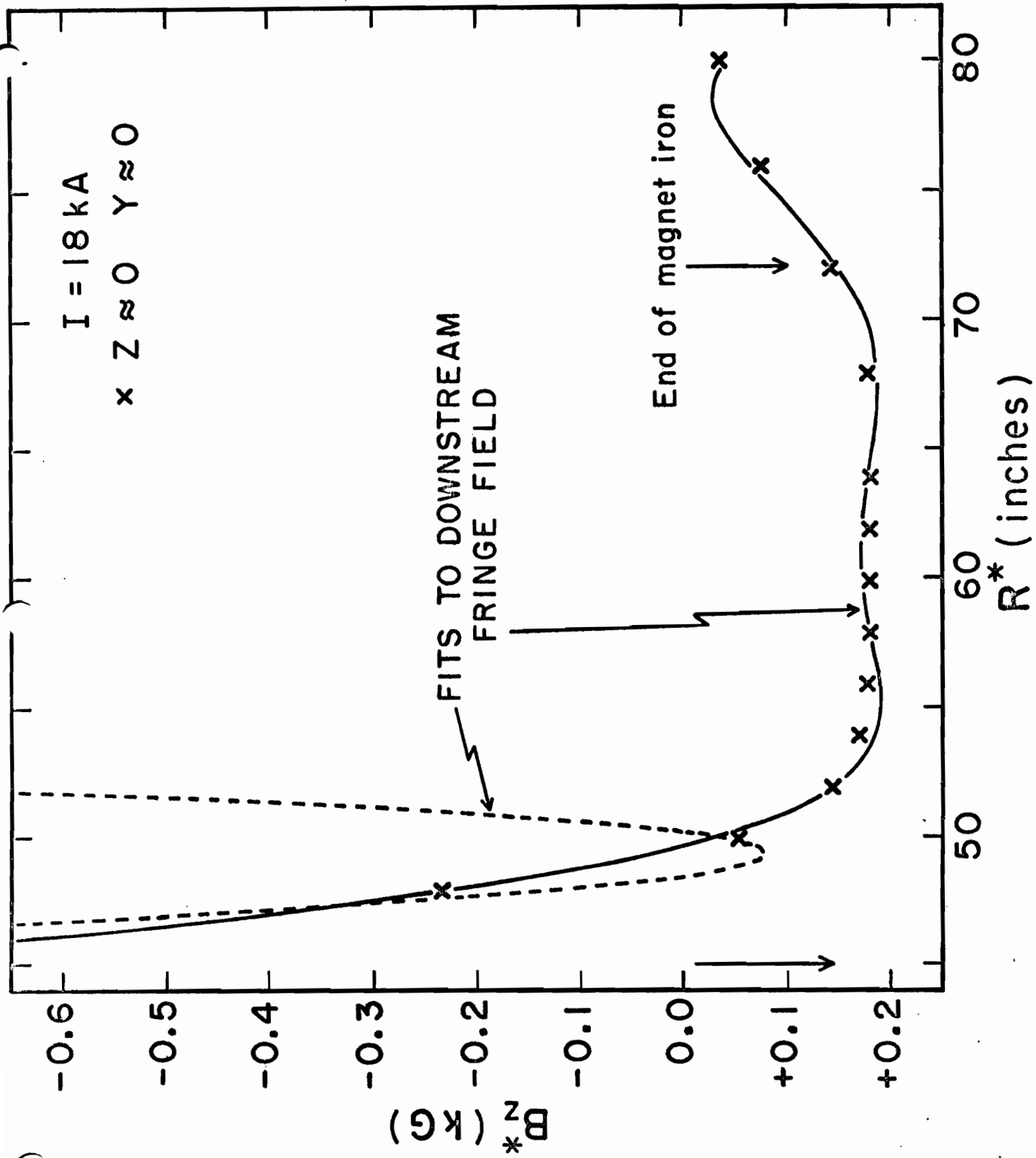


Figure 9b

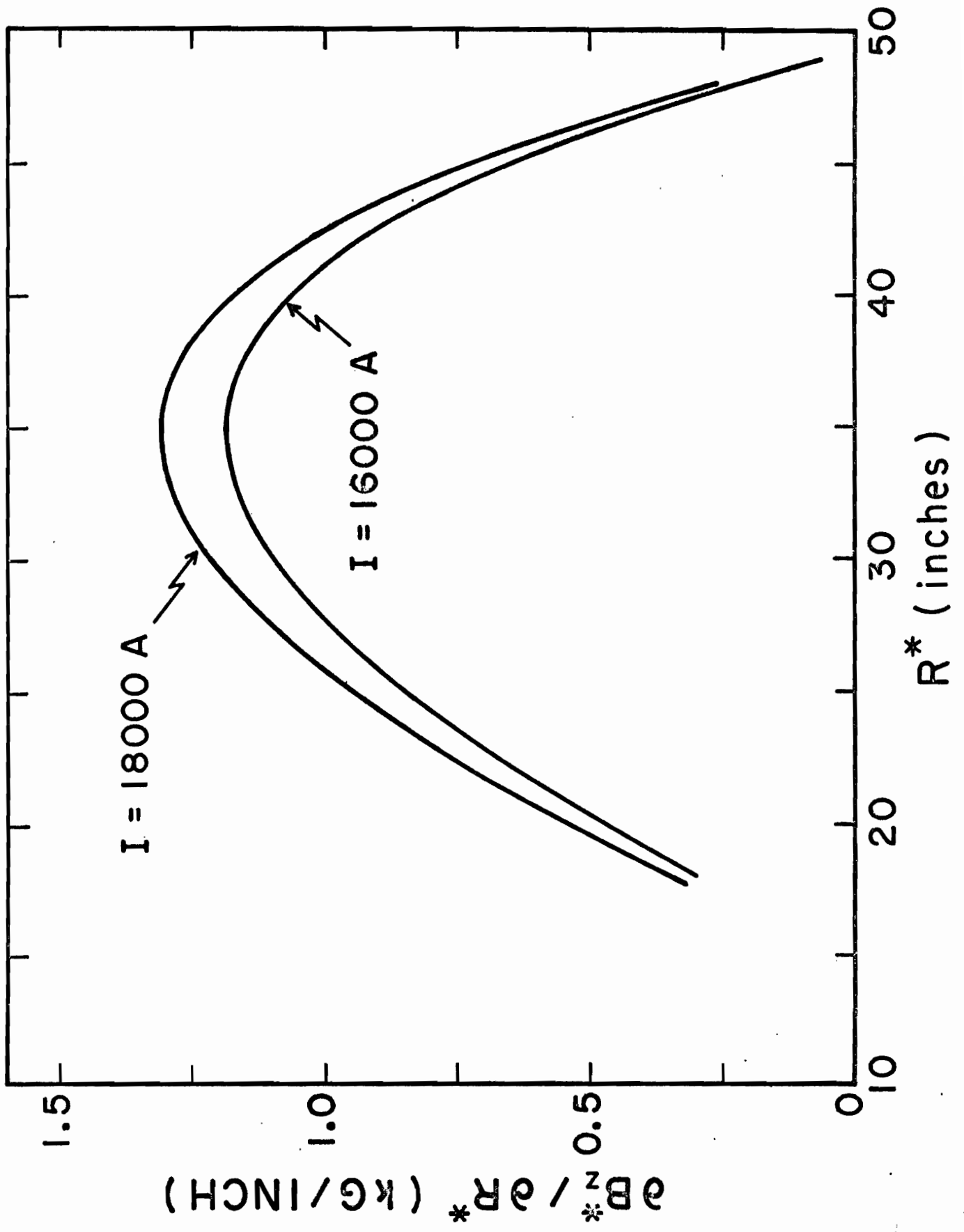
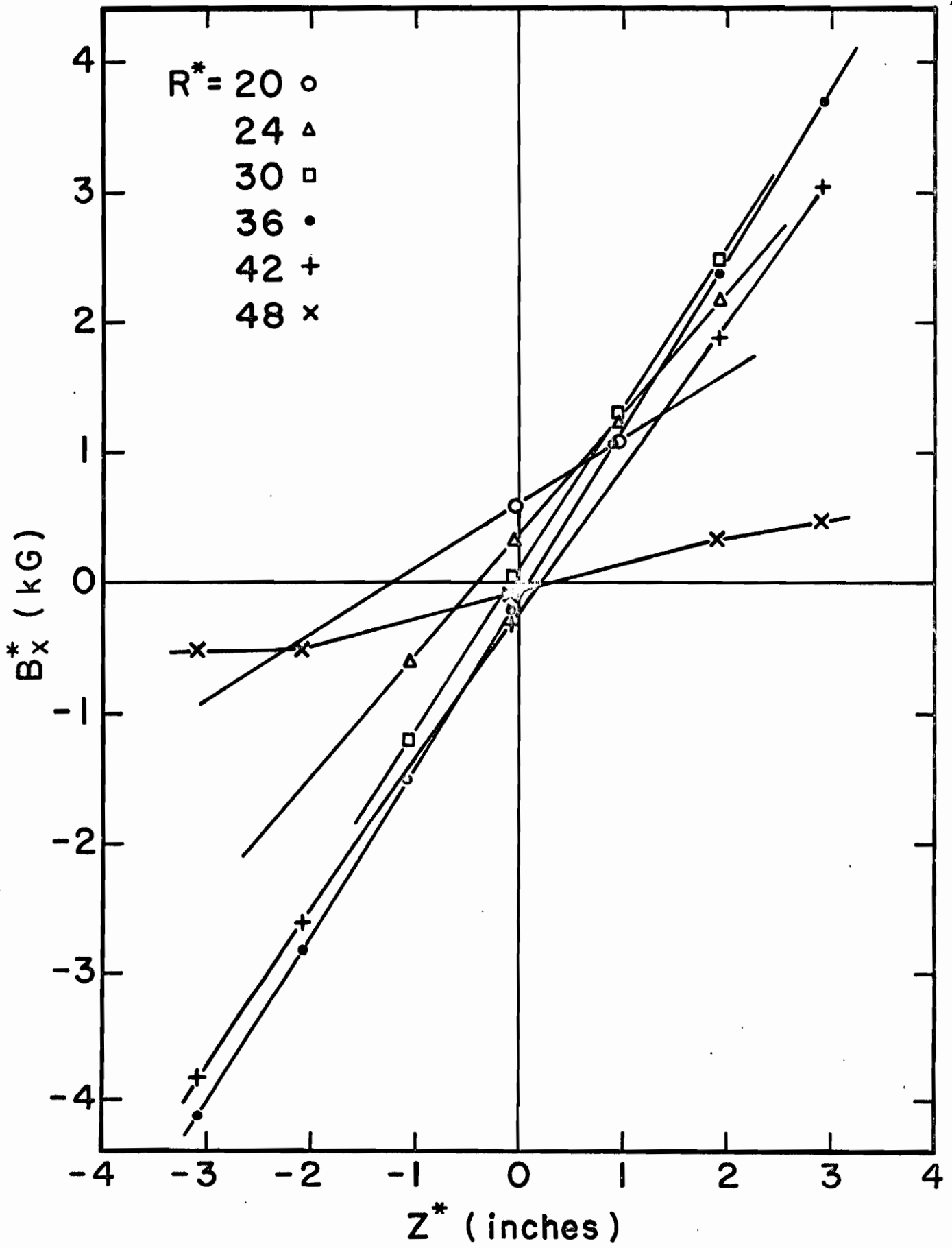


Figure 10



x EXPERIMENTAL VALUES  
I = 18000 A

$\frac{\partial B_x}{\partial z}$  (kg/inch)

R' (inches)

DERIVED FROM  
FIT TO  $B_z^*$  ( $R^*$ )

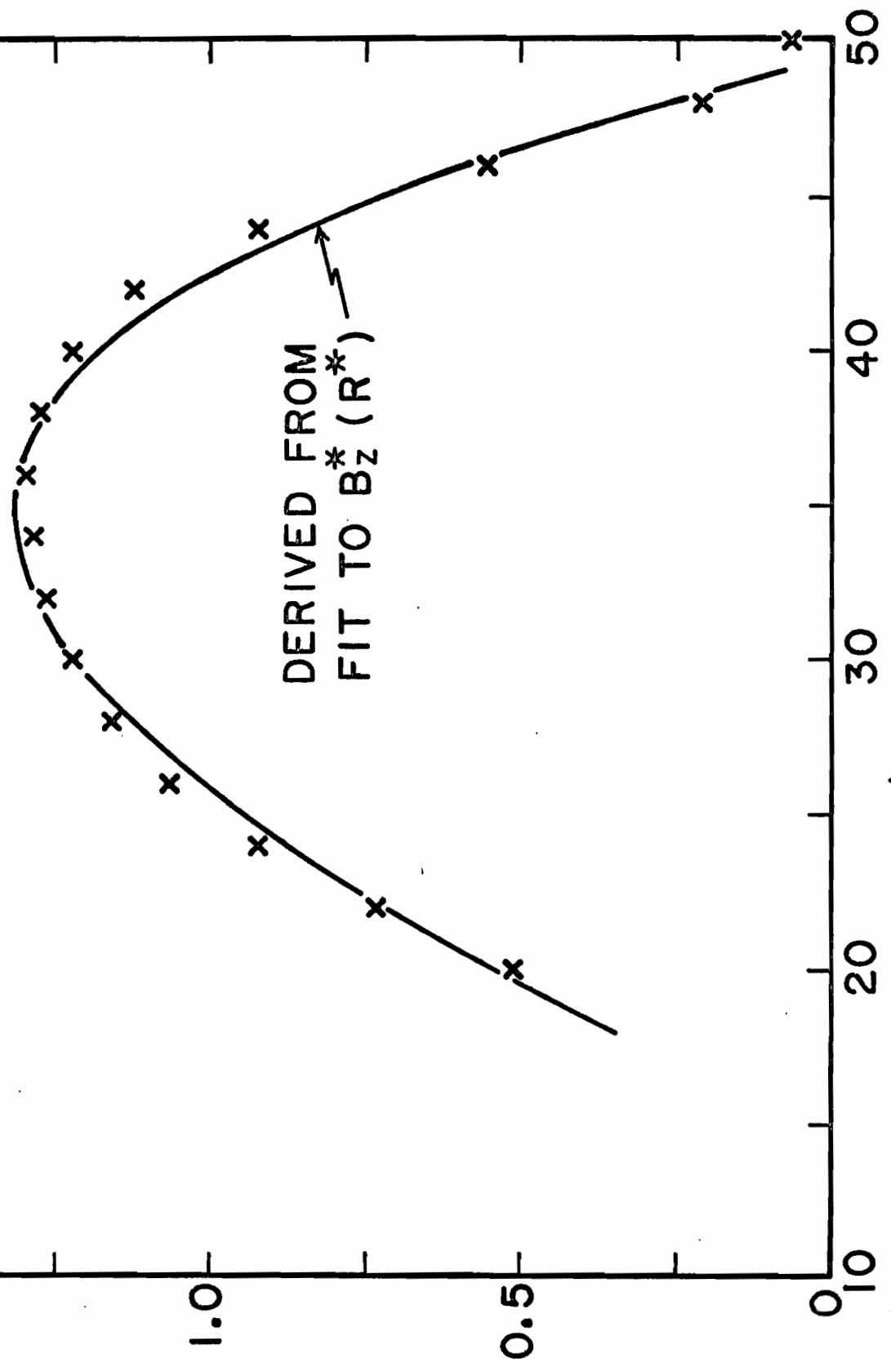
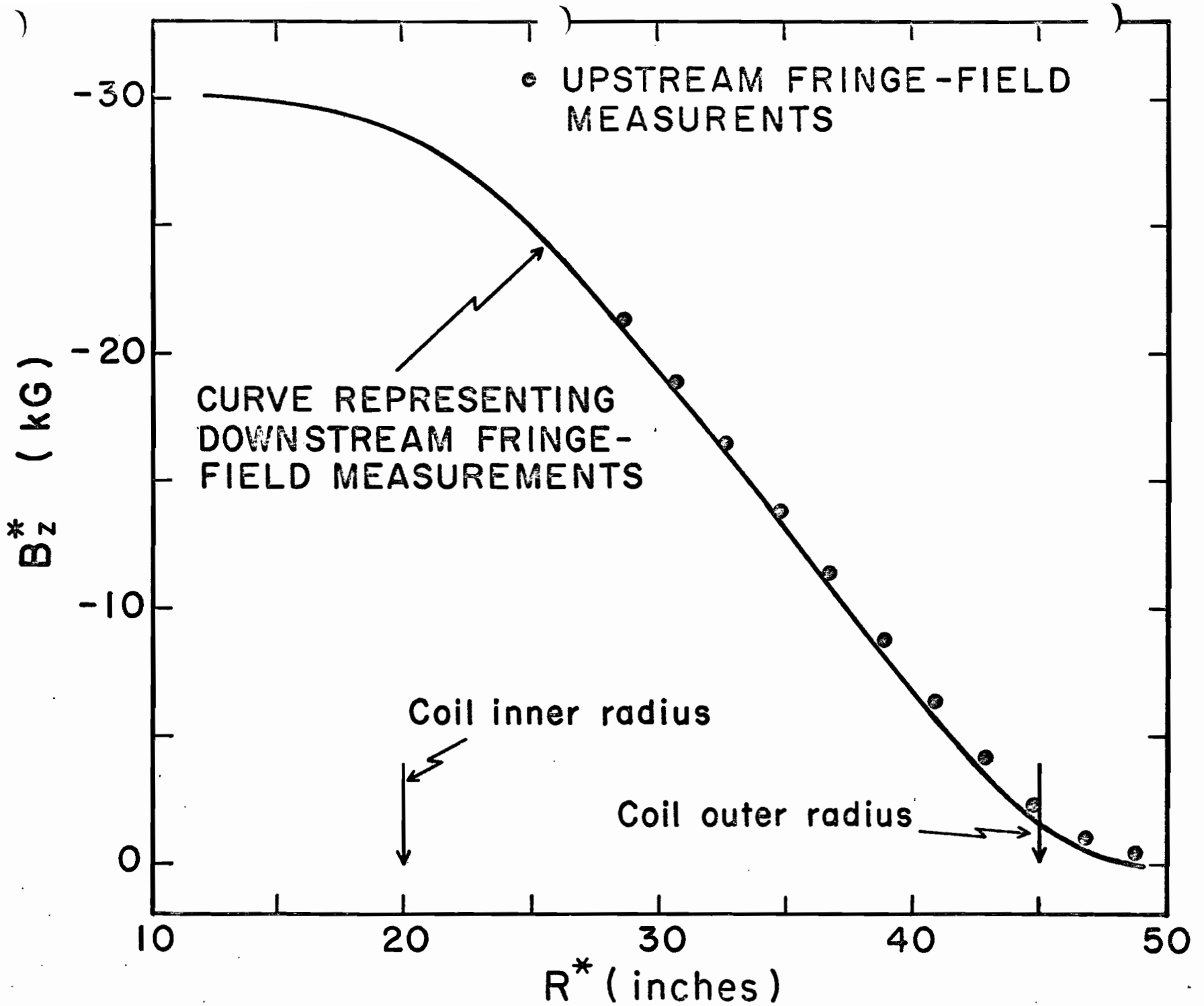
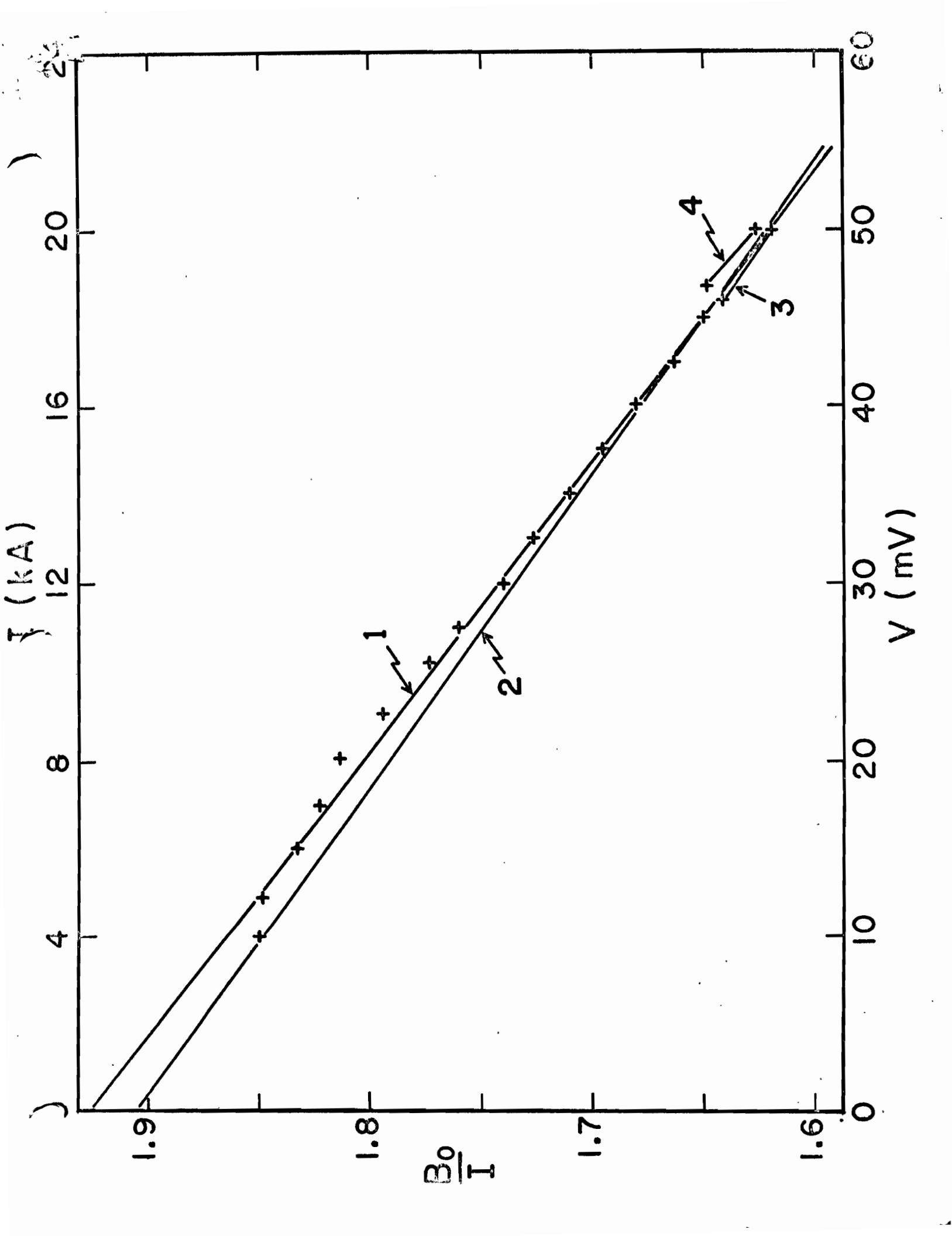
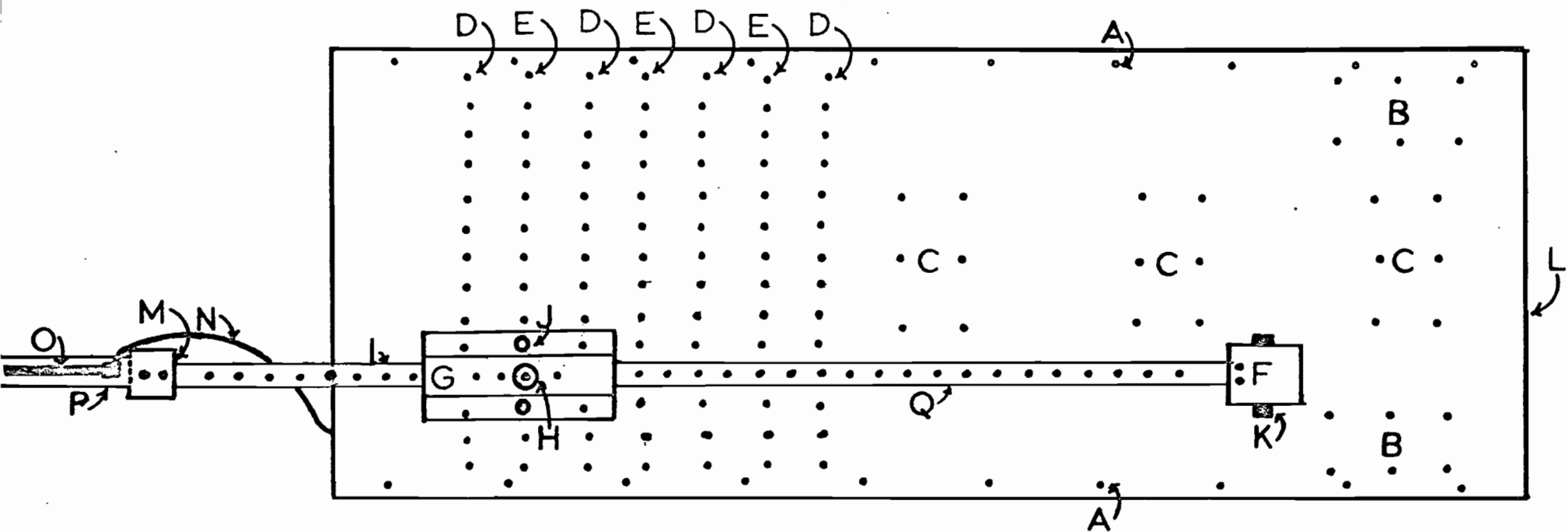


Figure 12

Figure 13



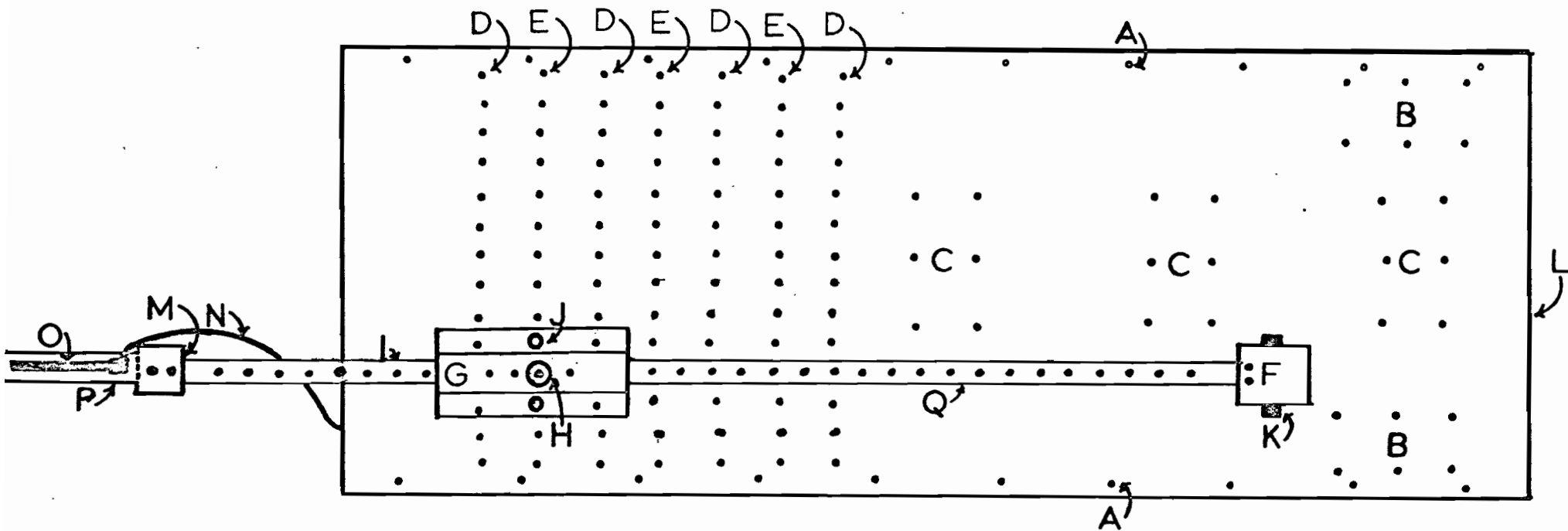




- A- Levelling Screws
- B- Auto-Collimating Block Hole Pattern
- C- Piston Measurement Hole Pattern
- D- X-Axis Alignment Hole Pattern
- E- Bearing Block Holddown Threaded Holes
- F- Guide Block and Counter Weight
- G- Bearing Block
- H- Alignment Pin
- I- Stainless Steel Rod
- J- Mounting Screws
- K- Roller Bearings
- L- 3/4" Tool Plate AL
- M- Probe Adapter
- N- Probe Cable
- O- Hall Probe
- P- Probe Holder
- Q- Z-Axis Alignment Holes

Figure 1

# 30" MAGNET FIELD MAPPING JIG



- A - Levelling Screws
- B - Auto-Collimating Block Hole Pattern
- C - Piston Measurement Hole Pattern
- D - X-Axis Alignment Hole Pattern
- E - Bearing Block Holddown Threaded Holes
- F - Guide Block and Counter Weight
- G - Bearing Block
- H - Alignment Pin
- I - Stainless Steel Rod
- J - Mounting Screws
- K - Roller Bearings
- L - 3/4" Tool Plate AL

- M - Probe Adapter
- N - Probe Cable
- O - Hall Probe
- P - Probe Holder
- Q - Z-Axis Alignment Holes

30" MAGNET FIELD  
MAPPING JIG

Figure 1

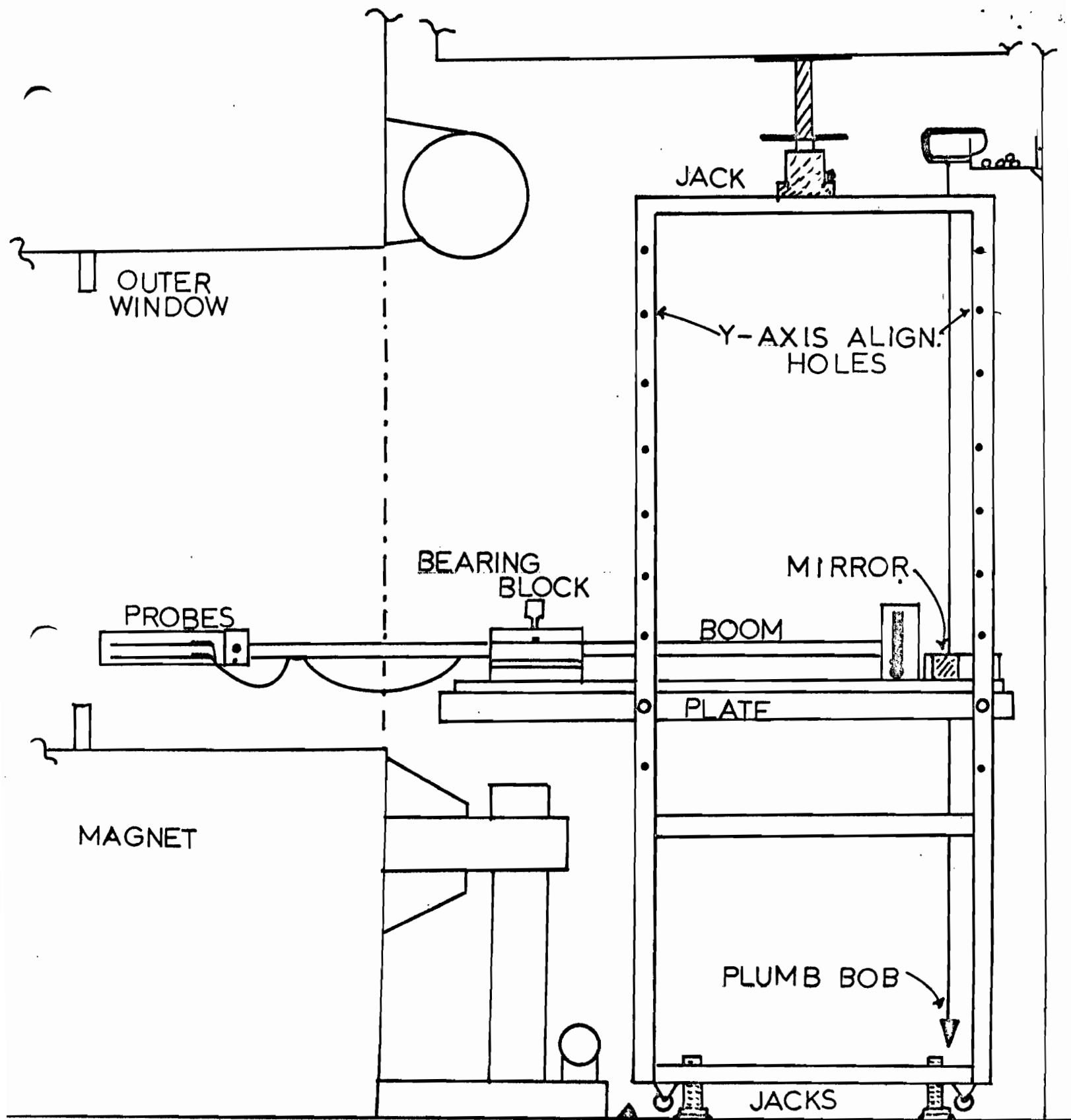


Figure 2

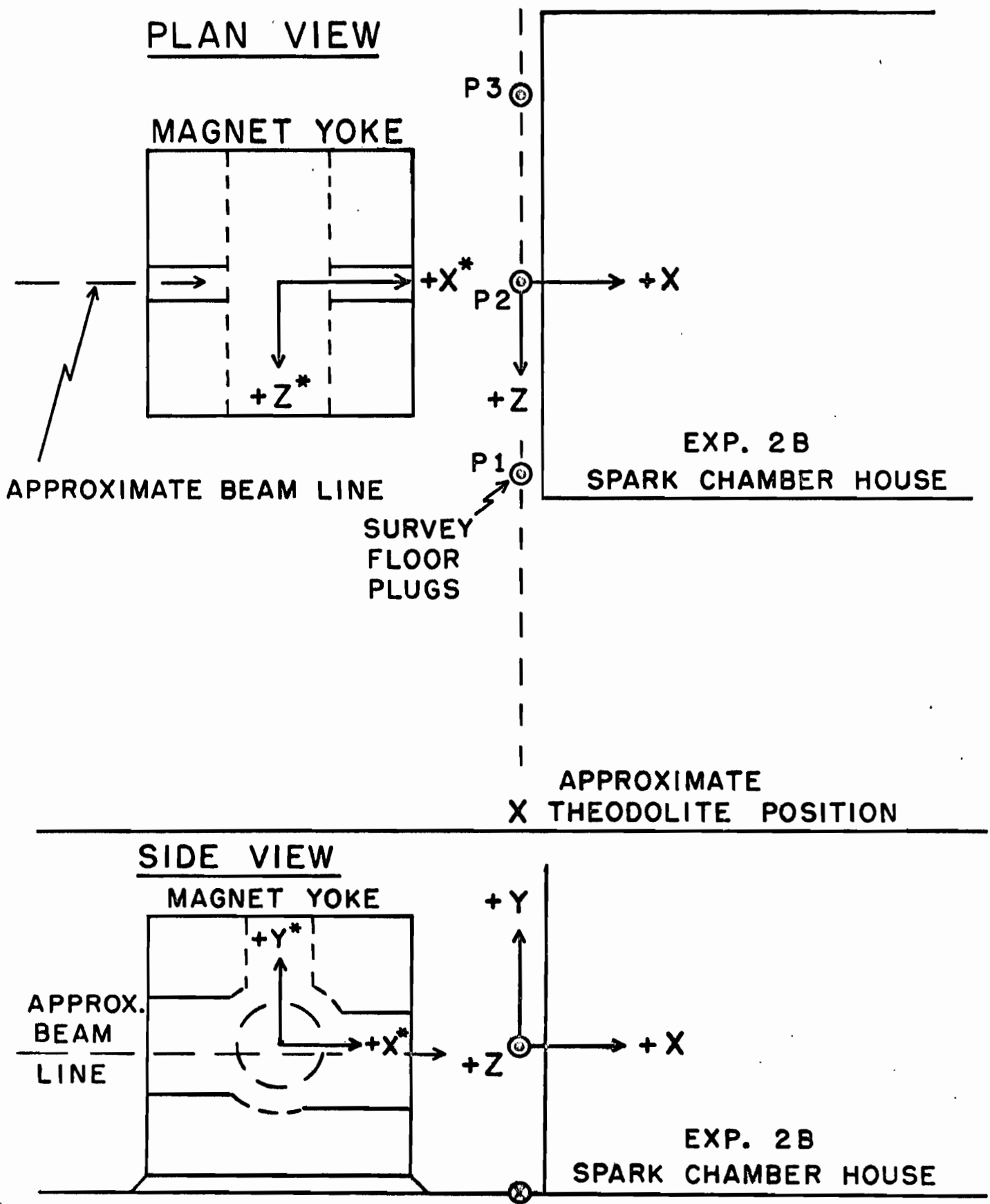


Figure 3

HORIZONTAL SECTION AT  $Y_0 = 0$

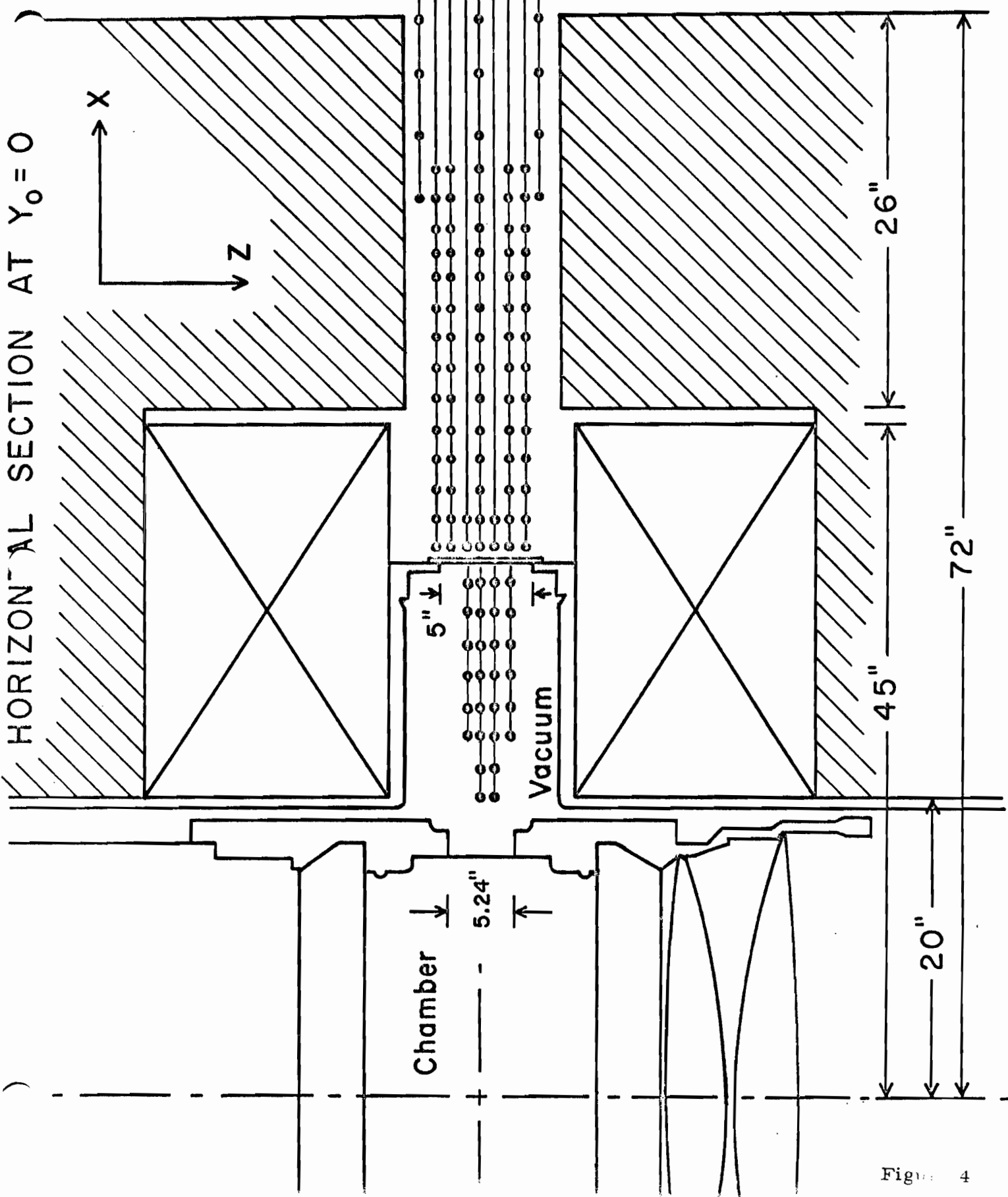


Figure 4

# 30" B.C. MAG. FIELD

Rechner - Biswas

## Measurement

Shift crew Enrichson, Thomson  
Biswas, Scholfield

Date 12/28/72  
Time started 13:25  
Time ended

Value of Y = 3.0  
Current = 45.05 amp  
105

X(Nom)	Z = -4		Z = -3		Z = -2		Z = -1		Z = 0		Z = 1		Z = 2		Z = 3	
	Bz	Bx	Bz	Bx	Bz	Bx	Bz	Bx	Bz	Bx	Bz	Bx	Bz	Bx	Bz	Bx
18																
20																
22																
24																
26																
28																
30																
32																
34																
36																
38																
40																
42																
44																
46																
48																
50																
52																
54																
56																
58																
60																
62																
60																
64																
68																
72																
76																
80																
84																

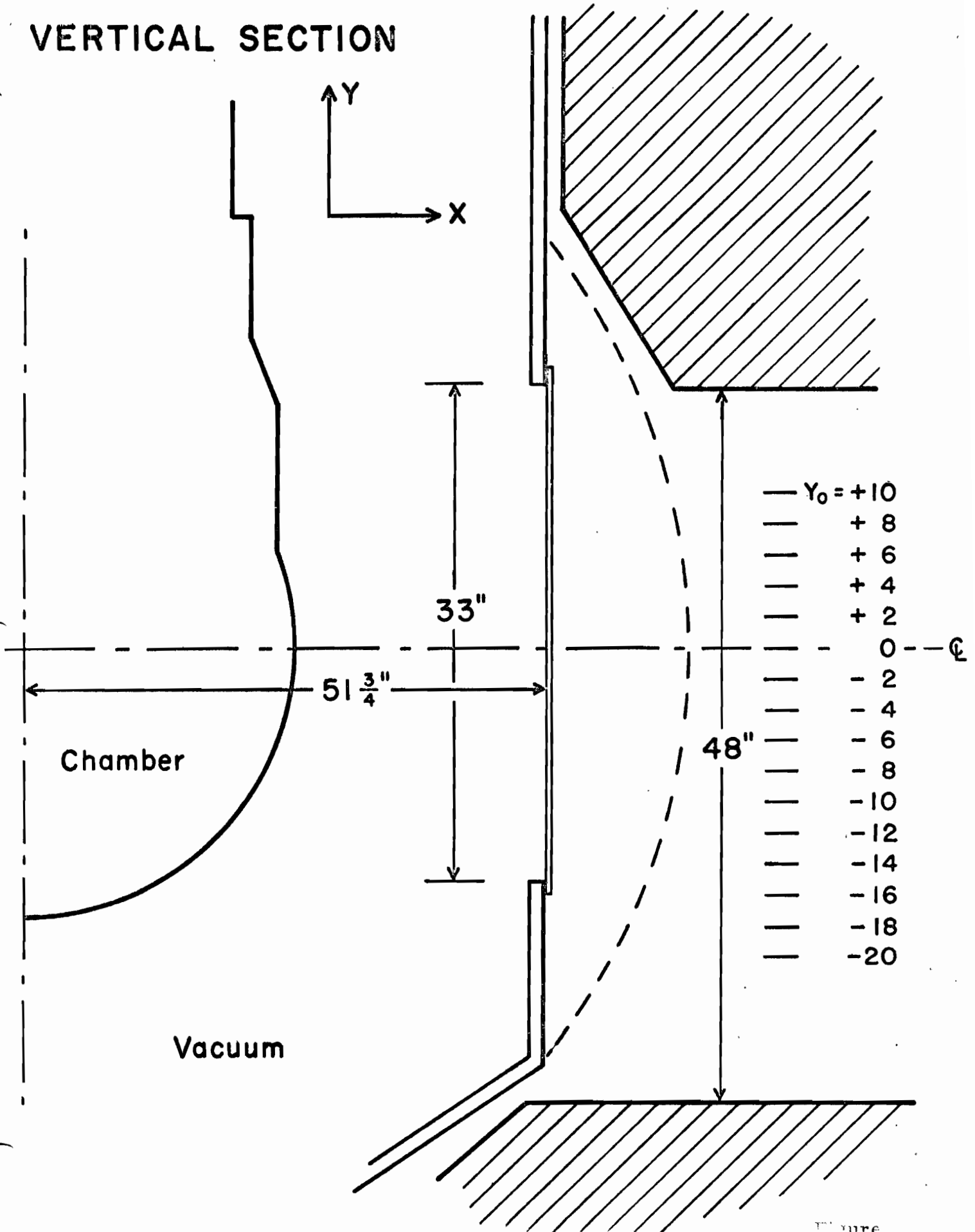
X-Probe REVERSE  
Z-Probe NORMAL

\*Range changed

T = 20°C

Figure 5

# VERTICAL SECTION



NO. HTL 8 - 0608

LINEARIZING RESISTOR,  $R_{lin} = \underline{500 \Omega}$

DATE: 12-13-72 INITIALS E.A.M.

INPUT RESISTANCE,  $R_{in} = \underline{1.35 \Omega}$

SENSITIVITY CONSTANT,  $\gamma_B = \underline{0.836 \text{ mV/kG}}$

OUTPUT RESISTANCE,  $R_{out} = \underline{\frac{.97}{1.2V} \Omega}$

CONTROL CURRENT,  $I_c = 100 \text{ mA}$

PROBE MODEL NO. HTL8-0608

HALL PROBE LINEARITY DEVIATION PLOT

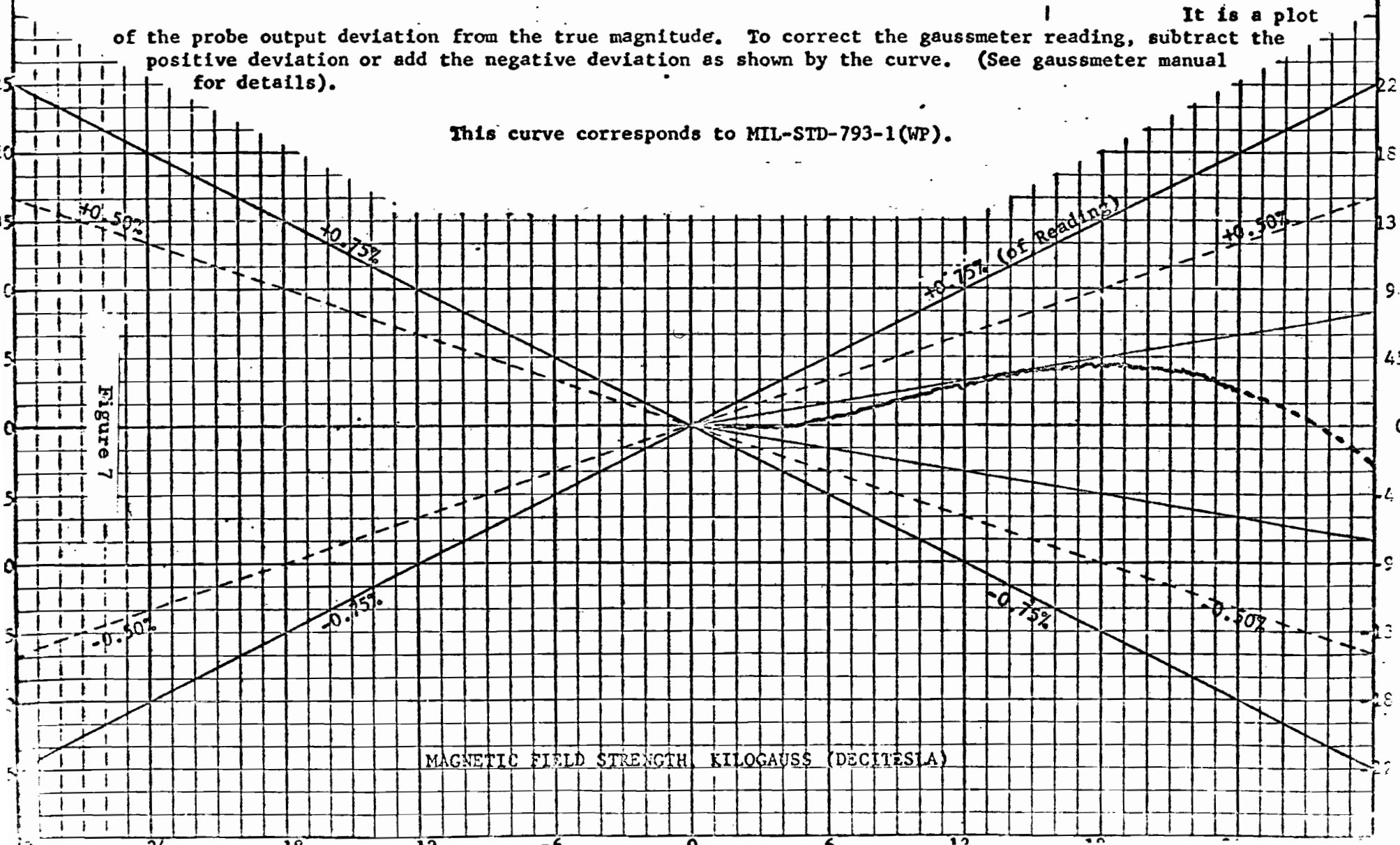
F. W. BELL, INC.  
COLUMBUS, OHIO U. S. A.  
DRAWING UA 2014

PROBE SERIAL NO. 77601

PROBE CAL. NO. 0.6748

It is a plot of the probe output deviation from the true magnitude. To correct the gaussmeter reading, subtract the positive deviation or add the negative deviation as shown by the curve. (See gaussmeter manual for details).

This curve corresponds to MIL-STD-793-1(WP).



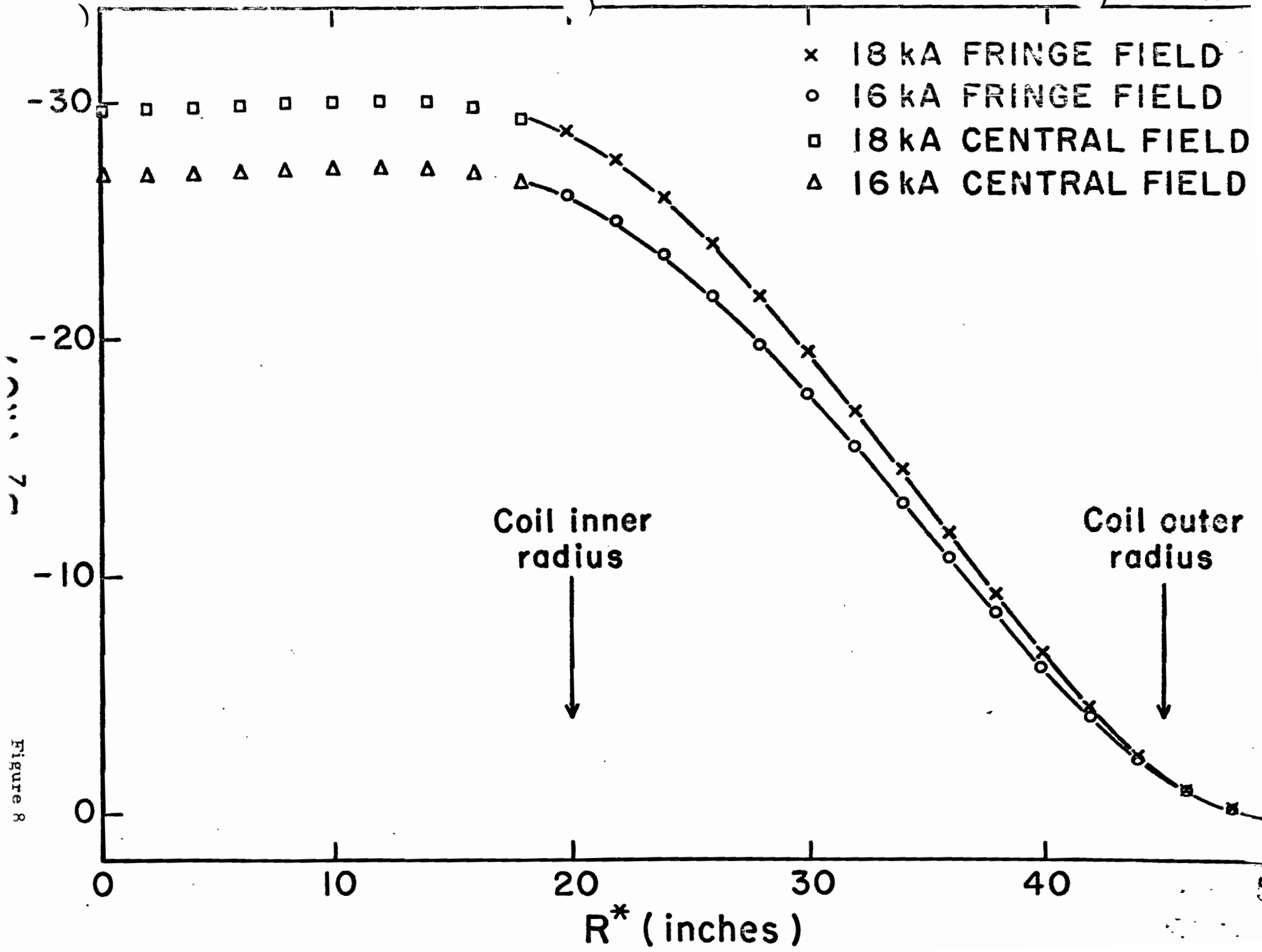


Figure 8

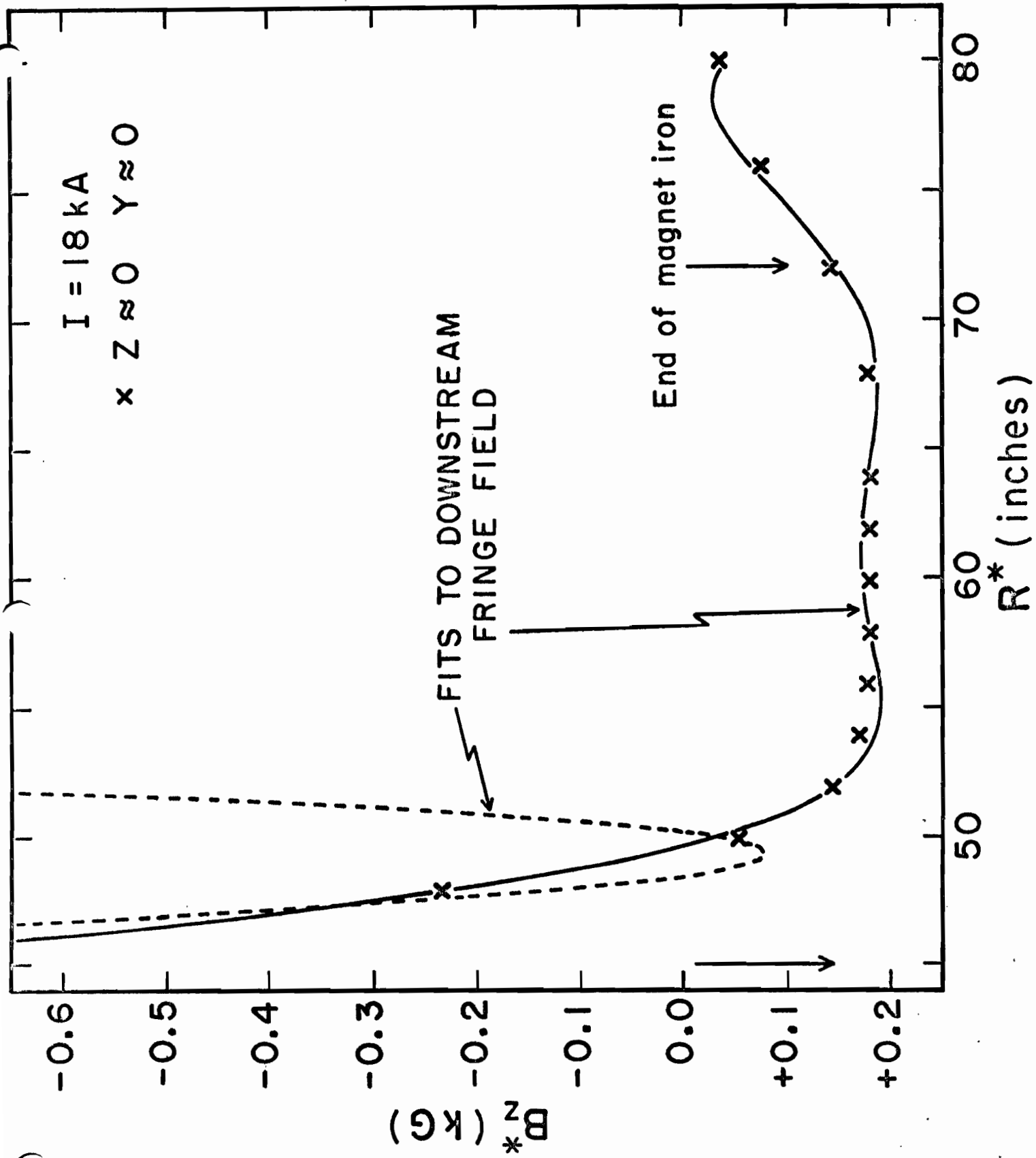


Figure 9b

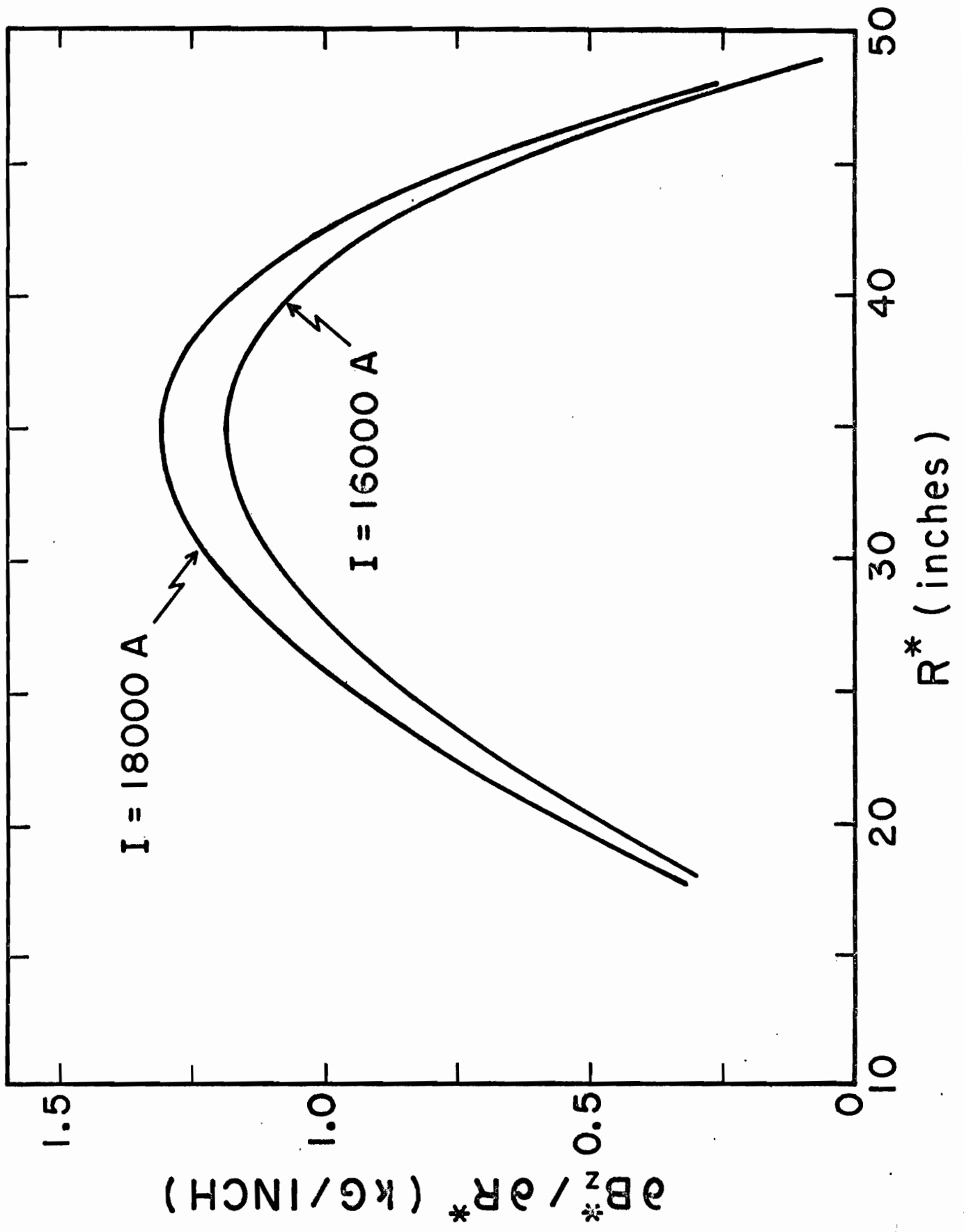
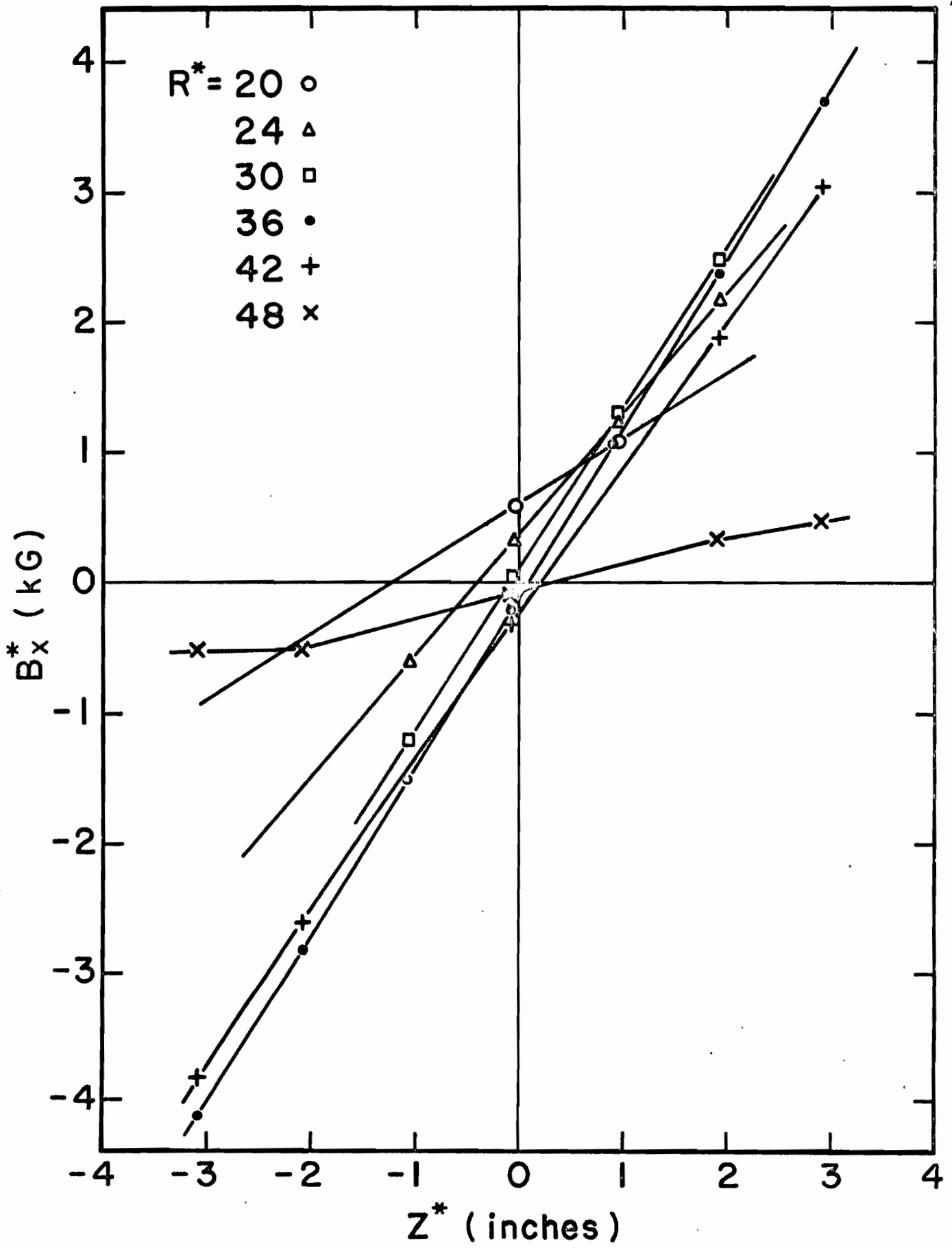


Figure 10



x EXPERIMENTAL VALUES  
I = 18000 A

$\frac{\partial B_x}{\partial z}$  (kg/inch)

R' (inches)

DERIVED FROM  
FIT TO  $B_z^*$  ( $R^*$ )

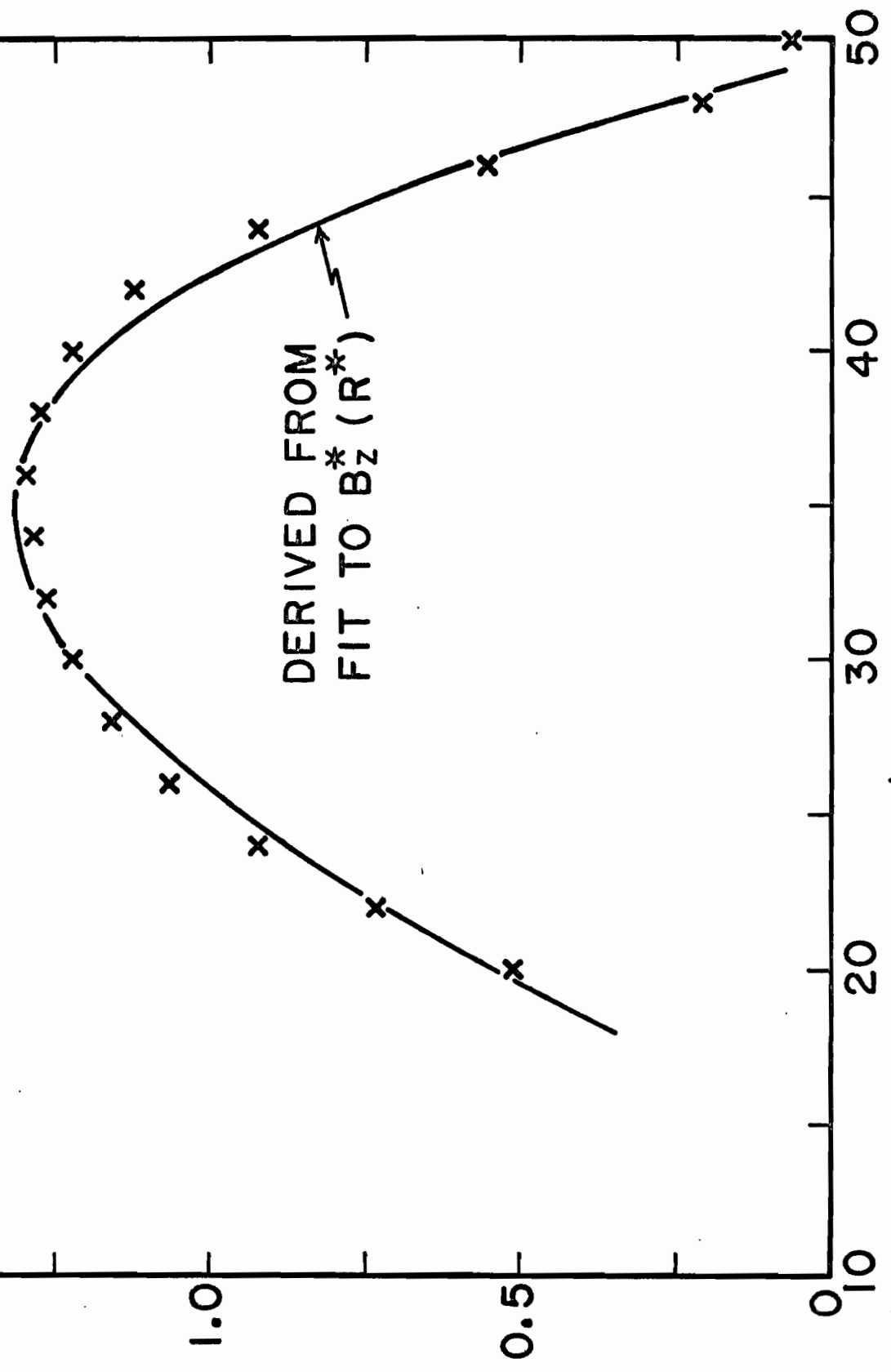


Figure 12

Figure 13

